Title	Critical phenomena of the metal-insulator transition in doped semiconductors using density functional theory and local density approximation
Author(s)	Harashima, Yosuke
Citation	大阪大学, 2013, 博士論文
Version Type	VoR
URL	https://hdl.handle.net/11094/27467
rights	
Note	

Critical phenomena of the metal-insulator transition in
doped semiconductors using density functional theory
and local density approximation

$$\left(\begin{array}{c}\text{密度汎関数理論と局所密度近似を用いた} \\ \text{半導体中での金属絶縁体転移の臨界現象に対する研究}\end{array}\right)$$

Yosuke Harashima

Department of Physics, Graduate School of Science,
Osaka University

February, 2013

Critical phenomena of the metal-insulator transition in doped semiconductors using density functional theory and local density approximation

$$\left(\begin{array}{c} 密度汎関数理論と局所密度近似を用いた \\ 半導体中での金属絶縁体転移の臨界現象に対する研究 \end{array} \right)$$

Yosuke Harashima

Department of Physics, Graduate School of Science,
Osaka University

February, 2013

Abstract

I report a numerical analysis of the critical behavior of the metal-insulator transition in a model of a disordered interacting system. In semiconductors a conductivity extrapolated to the zero temperature shows a metal-insulator transition as a function of doping concentration. This transition has been observed, for example, in silicon doped with phosphorus.

The impurities are randomly distributed in the system and the Anderson localization can play important roles in the metal-insulator transition. The critical behavior of the Anderson transition has been studied precisely. However, the critical exponent of the Anderson transition does not agree with the experimental results. This discrepancy can be attributed by an effect of electron-electron interaction. Relative importance of the roles played by disorder, which is arisen by randomly distributed impurities, and interaction between electrons, which, for example, screen the potential given by impurity ions, is an interesting problem.

The model considered in this study is, (i) positions of donor impurity ions are random, (ii) each impurity supplies one electron and the host material is dealt as an effective medium, (iii) the electrons interact with the impurity ions and with each other via long range Coulomb interaction.

I calculated the electronic ground state in a doped semiconductor using density functional theory and the local density approximation. In this study the spinless system is mostly considered for simplicity of the numerical analysis. Multi-fractal finite size scaling of the highest occupied Kohn-Sham orbital exhibit the critical impurity concentration $n_c \approx 1.1 \times 10^{18} \mathrm{cm}^{-3}$ and the critical exponent $\nu = 1.29(+0.08, -0.05)$. The obtained critical exponent differs from the result of the Anderson model of the non-interacting disordered system. This result indicates the importance of the electron-electron interaction in disordered systems.

Contents

Chapter 1

Introduction

Generally speaking, there are a lot of origins of disorder. Materials can have defects, distortion, impurities, or a system can be amorphous. The spatial translational symmetry of the system is broken by these factors and Bloch theorem is no longer applicable in such disordered systems. Quantum fluctuation from Bloch states occurs by the randomness of the system. In 1958, it was suggested that eigenfunctions can be localized as a result of the random scattering [1]. Since this disorder driven localization phenomena, which is called Anderson localization, was suggested, a lot of works about disordered systems have been done [2, 3, 4]. One of the important things related with the Anderson localization is the critical behavior of the metal-insulator transition driven by randomness of a system. When the randomness is weak the wavefunction can be extended over whole system. As the randomness becomes strong the localization of the wavefunction becomes significant. If the states are localized electrons can not move through the system, i.e. the system becomes an insulator.

The scaling behavior for β function defined as,

$$\beta(g) \equiv \frac{d \ln g}{d \ln L} \tag{1.1}$$

was studied to reveal the conductive phenomena [5] for the orthogonal class (the universality classes are explained in the next paragraph). g is a conductance and L is a system size. β in 1-, 2-, and 3-dimensional systems as a function of the conductance are shown in Fig. 1.1. If β function is negative,
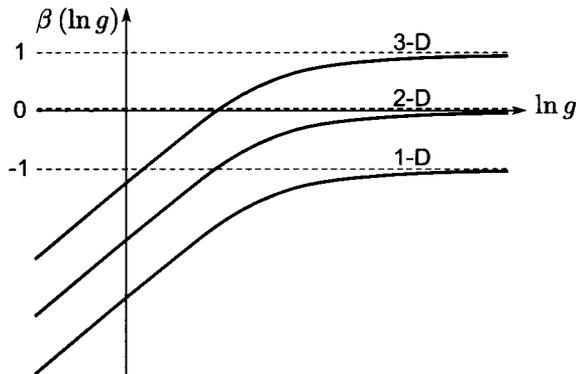
Figure 1.1: β as a function of the conductance, g [5].

the conductance decays to zero as the system size is increased, i.e. the system is an insulator. 1- and 2-dimensional systems are always an insulator. In 3-dimensional systems, both positive and negative region can be found and there can exist the metal-insulator transition. This scaling behavior was proved by numerical calculations [6, 7, 8].

The Anderson transition can be sorted out into three classes in terms of existence of time reversal (TRS) and spin rotational (SRS) symmetries (Table 1.1). The critical behaviors for each classes with some of the spatial

Table 1.1: Universality classes.

Class	TRS	SRS	Example of field
Orthogonal	O	O	
Unitary	×		Magnetic field
Symplectic	O	×	Spin-orbit coupling

dimensions are studied for several decades, for example, in Refs. [9, 10, 11]. The critical exponent for the metal-insulator transition in 3-dimensional orthogonal class was estimated precisely [12] using a simple model defined as,

$$\mathcal{H} = \sum_{\langle i,j \rangle} t\, \hat{c}_i^\dagger \hat{c}_j + \sum_i v_i \hat{c}_i^\dagger \hat{c}_i \qquad (1.2)$$

4

where t is a hopping coefficient and v_i is a random local potential. $\hat{c}_i$ $(\hat{c}_i^\dagger)$ is annihilation (creation) operator of a electron at site i. The tail states start to be localized as the randomness being braced up and there are extended states in the middle of the band as shown in Fig. 1.2. The borders separating the extended and localized states are mobility edges. When the mobility edge crosses Fermi energy as the system becomes more random the metal-insulator transition occurs. Ref. [12] showed the critical exponent $\nu = 1.57(\pm 0.02)$
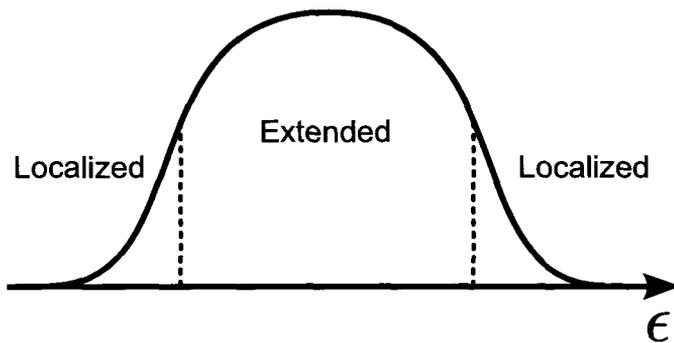

Figure 1.2: Schematic representation of the averaged density of states of Eq. (1.2). The mobility edge is shown as a dashed vertical line. The mobility edge moves from the band tail towards the center as randomness is braced up.

which describes the divergence of the localization (correlation) length at the cricital point.

$$\xi \propto \left| \frac{W - W_c}{W_c} \right|^{-\nu} \tag{1.3}$$

where W and W_c are a parameter describing randomness and its critical value, respectively. The analysis in Ref. [12] is based on the transfer matrix method [8, 7]. The critical value of the transition is not universal, but the critical exponents should be independent on details of a system. Indeed, the critical exponents does not depend on, for example, the distribution functions for the random potential [12] and the boundary conditions [13]. Because the characteristic length scale is infinity at the critical point, the wavefunctions show characteristic behavior. The distribution of the wavefunction intensity at the critical point has multi-fractality [14, 15]. This can be generalized for the critical exponent calculations [16, 17]. The critical exponent resulted from

5

generalized multi-fractal analysis is $\nu = 1.590(+0.012, -0.011)$ and this value is consistent with the above value obtained using transfer matrix method. These studies are based on a single particle representation. How the critical behavior of the metal-insulator transition changes by electron-electron interaction is an attractive problem.

To study the critical behavior of the transition with both disorder and electron-electron interaction one can consider the metal-insulator transition in impurity doped semiconductors. In semiconductors a zero temperature metal-insulator transition is observed as a function of doping concentration. For samples with concentrations below a critical concentration, the conductivity extrapolated to zero temperature is found to be zero. For samples with concentrations exceeding this critical concentration, the zero temperature limit of the conductivity is finite [18, 19]. The zero temperature conductivity σ in the metallic phase grows as

$$\sigma\left(n_D\right) \propto \left|\frac{n_D - n_c}{n_c}\right|^{\mu} \tag{1.4}$$

where n_D and n_c are the impurity concentration and the critical concentration, respectively. μ is the conductivity critical exponent. From Wegner's scaling law [20] one can find the relationship between μ and ν using a dimension of the system d.

$$\mu = \left(d - 2\right)\nu \tag{1.5}$$

and $\mu = \nu$ in 3-dimensional systems. The metal-insulator transition in doped semiconductors has been also observed as a function of uniaxial stress [21, 22] to tune the impurity concentration. Experimental values for μ were argued between ≈ 0.5 [18, 21] and ≈ 1.0 [19, 22]. This difference can be attributed from a range of the critical region [19, 22, 23, 24]. When one restricts the fitting analysis within very narrow concentration region in uncompensated samples, the result with such narrow region shows $\mu = 1.2 \pm 0.2$ [23]. (In Ref. [23] ν is estimated by considering the localization length directly and the results exhibit a similar discrepancy.) Those critical regions can be separated by measuring the sign of $d\sigma/dT$ (T is temperature) in the metallic phase [19, 24]. The scaling analysis within narrow region where $d\sigma/dT > 0$ leads to $\mu \approx 1.0$. The critical parameters obtained for uncompensated samples within the narrow region shows good agreement with the results for

6

compensated samples. Thus, the critical behavior in uncompensated samples can be resulted from small unavoidable doping compensation [23]. However, there is a fact that the scaling analysis is justified within close region of the scaling variables. If there exists critical region near a critical point, the scaling analysis within surrounding region will not work properly. The argument about this problem is still required.

Table 1.2: The critical exponent of the experimental results. These results were obtained from concentration tuned (c-tuned) and stress tuned (s-tuned) schemes. Dependence of the range of concentration or stress, wide (W) and narrow (N), is also shown.

	μ	Range	Sample	Ref.
c-tuned, uncompensated	0.55 ± 0.1		Si:P	[18]
	0.64	W	Si:P	[19]
	0.50 ± 0.04	W	Ge:Ga	[23]
	1.3	N	Si:P	[19]
	1.2 ± 0.2	N	Ge:Ga	[23]
s-tuned, uncompensated	0.48 ± 0.07		Si:P	[21]
	1.0 ± 0.1	N	Si:P	[22, 24]
c-tuned, compensated	1.01 ± 0.04		Ge:Ga	[23]

The universality of the metal-insulator transition has been confirmed in several models (see Table 1.3). A topologically disordered system is a system that electron propagates through randomly distributed scattering points and the hopping intensity is determined by distance between the scattering points [25]. In comparison with experimental results, the results of numerical analysis in non-interacting disordered systems, for example, $\nu = 1.57$ [12] for Anderson model using transfer matrix method, do not agree. A most likely candidate of an origin of the difference is the electron-electron interaction. This discrepancy can indicate the importance of the electron-electron interaction in disordered systems.

One can interpret a situation of this metal-insulator transition as following. Suppose donor impurities are doped in a semiconductor. If electrons

Table 1.3: The critical exponent of the numerical results for 3-dimensional orthogonal class. The results of the Anderson model with transfer matrix (TM) and multi-fractal analysis (MFA) are shown separately.

	ν	Ref.
Anderson model (TM)	1.57 ± 0.02	[12]
Anderson model (MFA)	1.590 (+0.012, -0.011)	[17]
Topologically disordered model	1.61 (+0.07, -0.06)	[25]

supplied from the donors screen an impurity potential, Thomas-Fermi screening length, r_{TF}, can be calculated as a function of the electron concentration (this is equal to the impurity concentration).

$$r_{\text{TF}} \equiv \frac{1}{2} \left(\frac{\pi}{3} \right)^{\frac{1}{6}} a_B^{*\frac{1}{2}} n_D^{-\frac{1}{6}} \tag{1.6}$$

a_B^* is an effective Bohr radius given by using the effective mass m_e^* and dielectric constant ε_r.

$$a_B^* = \frac{\varepsilon_r}{m_e^*} a_B \tag{1.7}$$

For low impurity concentration, the screening is weak. When the screening becomes so weak that $r_{\text{TF}} > a_B^*$, an electron will be trapped on an impurity and the description about the screening length of Eq. (1.6) is no longer correct. When the impurity concentration becomes so high that $r_{\text{TF}} < a_B^*$, an electron can not be localized on an impurity. Between these limits,

$$r_{\text{TF}} \approx a_B^* \quad \Rightarrow \quad n_c^{\frac{1}{3}} a_B^* \approx 0.25 \tag{1.8}$$

there should exists the metal-insulator transition [26]. The metal-insulator transition observed in the sets of some semiconductors and impurities shows the universal behavior [27] and Eq. (1.8) well agrees with those experimental results.

$$n_c^{\frac{1}{3}} a_B^* = 0.26 \tag{1.9}$$

One can expect the metal-insulator transition occurs with same physical mechanisms on effective mediums even though there are some small deviations from the universal behavior.
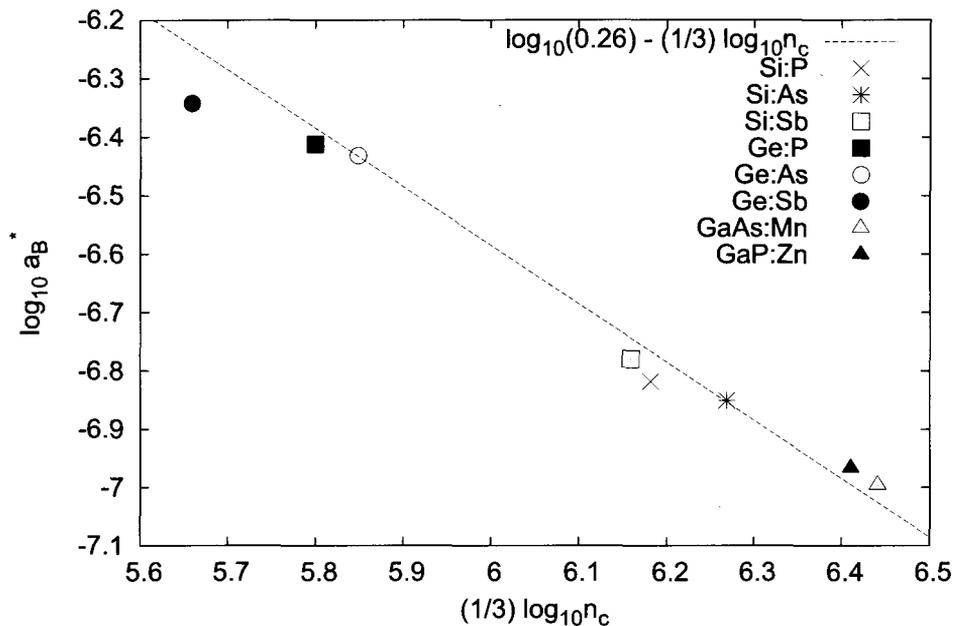
Figure 1.3: The critical concentrations and effective Bohr radius for some materials by log-scale (data are extracted from Ref. [27]).

When an impurity is doped, from an analogy of a system describing a hydrogen atom in an effective medium, an impurity level appears near below a conduction band. If some donors are doped the impurity levels become an impurity band. The Coulomb interaction between the electrons leads to that the impurity band is split into upper and lower Hubbard bands. In this case one can adopts the description for low impurity concentration in the previous paragraph. Without any compensation by acceptor impurities, the system is half-filled and it becomes an insulator. If the impurities align, for example, on the simple cubic lattice, an anti-ferromagneic order appears [28]. As more impurities are doped, the width of the impurity band gets larger and the Hubbard gap closes at some impurity concentration. Now the screening becomes strong and electrons start to move between impurities. If the effect of the disorder is neglected the metal-insulator transition is associated with this band closing [29, 30, 31]. This is a first order phase transition due to the electron-electron interaction [28]. The magnetic property is also interesting near the metal-insulator transition. As the system becomes from an insulator
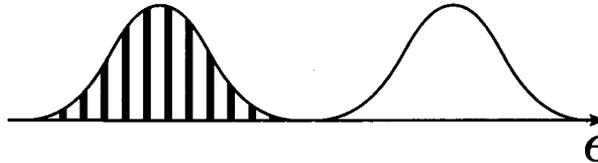
9

Figure 1.4: For low impurity concentration the upper and lower Hubbard bands are separated. Shaded region represents occupied states.

to metal, the magnetic moment changes discontinuously to smaller value but it is still finite value [29]. If the true metal-insulator transition in doped semiconductors were a discontinuous transition, the description about critical parameters would be wrong.
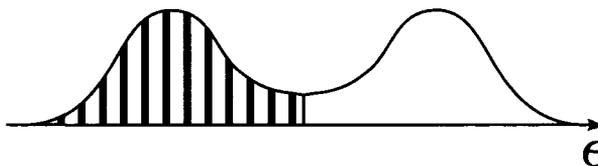
Figure 1.5: As the impurity concentration is increased, the band width broadens. Finally the upper and lower Hubbard bands merge.

Note that the donor impurities are distributed randomly in real space and the effect of disorder arising from this random distribution i.e. the possibility of the Anderson localization can be important for this metal-insulator transition. One of the evidences is a fact that this Anderson transition is a continuous transition. In disordered systems averaged density of states decays smoothly at band edges and a band tail appears [30]. Eigenstates in

10

this band tail can be Anderson localized states. This localized states do not contribute the conductivity. Even though the band merges and the density of states at Fermi level is not zero, the eigenstates around Fermi level can be the Anderson localized states and the system can be still an insulator. When more impurities are doped after the band gap closing the metal-insulator transition occurs. There are many proposals for this metal-insulator transition. For example, in Refs. [30] and [32] the multi-valley effect and clustering impurities were discussed. Refs. [33, 34, 35, 36] suggested the importance of the effect of the electron-electron interaction in the metal-insulator transition. The relative importance of the roles that the electron-electron interaction and disorder play in this metal-insulator transition, especially for its critical behavior, is still not clear.

The problem including both disorder and electron-electron interaction is difficult to solve in a direct way. One of commonly used framework is density functional theory [37, 38, 39]. Density functional theory is widely used in the first principles calculation. This theory proves an important fact that any physical quantities are a functional of a ground state density. This fact means that if one can obtain a ground state density it is possible to calculate any physical quantities without many body wavefunctions. Using density functional theory one can replace a many body problem by a single particle problem in an auxirialy system so that the ground state density of the single particle problem becomes same as that of the original many body problem [40, 38, 39]. The equations derived in the auxirialy system is called Kohn-Sham equations.

The most important example for this scheme is a homogeneous system. In homogeneous systems a ground state density is expected to be an uniform density. However, a many body wavefunction is no longer a single Slater determinant consisting of single particle plane wave states and it is given by linear combination of the Slater determinants. On the other hand, a wavefunction in an auxirialy system is the single Slater determinant of plane waves. These two wavefunctions lead to the same uniform density and the ground state energy must be same in both problems. In Kohn-Sham scheme the contribution from the exchange and correlation energy, which corrects the energy in the auxirialy system, is given as a functional of the density.

11

Kohn-Sham equations have a problem with the exchange and correlation energy. The exact density functional for these contributions is not known. The most commonly used approximation is the local density approximation [38, 39]. This approximation is that the exchange and correlation energy is estimated by using a functional of the homogeneous system with the local density.

The purpose of this study is to analyse the critical behavior of the metal-insulator transition taking into account both the disorder and electron-electron interaction. I studied the details of the metal-insulator transition in a doped semiconductor using numerical calculation. I simulated the case that electron spins are restricted to be polarized completely, i.e. the spinless case, and the case without this restriction. From the results multi-fractal exponents are estimated and finite size scaling of the multi-fractal exponents exhibits existence of the metal-insulator transition [41].

Chapter 2

Method

For convenience of the numerical analysis, I used the atomic units shown in Appendix A. Physical quantities are given using Å, cm^{-3}, eV, explicitly.

2.1 Model for disordered interacting system

I consider that the donor impurities are doped in a host semiconductor crystal and these impurities are randomly distributed in real space. There is the universal feature that the critical impurity concentration of the metal-insulator transition, n_c, in doped semiconductors is approximately determined by the effective Bohr radius (Eq. (1.7)) in the host semiconductor crystal [27]. The experimental results suggest the universal relationship between the effective Bohr radius and critical concentration below.

$$n_c^{\frac{1}{3}} a_B^* = 0.26 \qquad (2.1)$$

This fact means that the contribution to this metal-insulator transition is mainly from the electrons which behave as a particle defined with the effective mass m_e^* and dielectric constant ε_r of the host semiconductor. Since I consider phosphorus as the impurity and silicon as the host semiconductor the effective mass and dielectric constant are
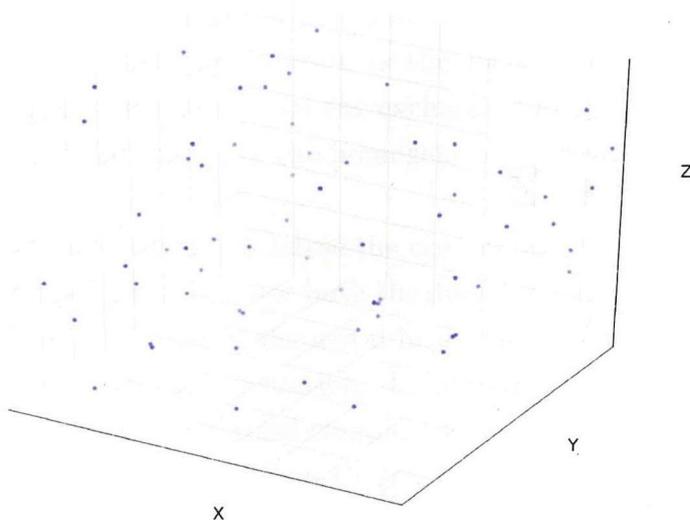
$$m_e^* = 0.32 \, , \ \varepsilon_r = 12.0 \qquad (2.2)$$

Figure 2.1: The randomly distributed impurities are shown as blue points. This figure is one sample for $N = 65$, $L = 400$ Å, $n_c = 1.02 \times 10^{18} \mathrm{cm}^{-3}$.

From the universal relationship of Eq. (2.1), the critical concentration of phosphorus doped silicon can be predicted from Eqs. (1.7) and (2.2) as

$$n_c = 2.25 \times 10^{18} \ \mathrm{cm}^{-3} \tag{2.3}$$

The critical concentration in the experiment for silicon doped with phosphorus is [24],

$$n_c = 3.52 \times 10^{18} \ \mathrm{cm}^{-3} \tag{2.4}$$

and Eq. (2.1) can be estimated by using Eqs. (1.7), (2.2) and (2.4),

$$n_c^{\frac{1}{3}} a_B^* = 0.30 \tag{2.5}$$

The deviations from the universal relationship could have lost when the effective medium is assumed instead of considering the true semiconductor. Even though there are such deviations for each material it is not so important in this study and I concentrate on the universal behavior.

Since I have in mind silicon doped with phosphorus I assume that each donor supplies one electron and each impurity ion has a net charge of $+e$.

From the universal relationship described above, it is expected that the electrons supplied from donor impurities operate the metal-insulator transition. I concentrate on electronic states in an effective medium with the effective mass and dielectric constant of the host semiconductor. One can consider an electron moving with the effective mass. The kinetic energy term can be expressed as, (see Appendix B.1)

$$-\frac{1}{2m_e^*}\nabla^2 \tag{2.6}$$

The electron interacts with the donor impurities through the screened Coulomb interaction given in the effective medium. I assume that the Coulomb interaction in the effective medium is given by [42, 43]

$$-\frac{1}{\varepsilon_r}\frac{1}{|\boldsymbol{r}-\boldsymbol{R}|} \tag{2.7}$$

where $\boldsymbol{r}$ and $\boldsymbol{R}$ are a position of an electron and donor impurity ion, respectively. The random spatial distribution of the donors thus produces a random potential in which the electrons move. At the same time the electrons interact with each other via the Coulomb interaction in the effective medium. In this study, I assume that the valence electrons of the host medium screen the electrons supplied from donor impurities as the impurity ions are screened. The Hamiltonian of this system is

$$\mathcal{H} = -\frac{1}{2m_e^*}\sum_{i=1}^{N}\nabla_i^2 - \frac{1}{\varepsilon_r}\sum_{i,I=1}^{N}\frac{1}{|\boldsymbol{r}_i-\boldsymbol{R}_I|} + \frac{1}{2\varepsilon_r}\sum_{i\neq j}^{N}\frac{1}{|\boldsymbol{r}_i-\boldsymbol{r}_j|} + \frac{1}{2\varepsilon_r}\sum_{I\neq J}^{N}\frac{1}{|\boldsymbol{R}_I-\boldsymbol{R}_J|} \tag{2.8}$$

The first term is the kinetic energy of the electrons. The second term describes the interaction of the electrons with the donor impurity ions. Here R_I is a random variable. N is a number of impurity ions and there are an equal number of electrons since the system must be neutral. The third and fourth term describe the interaction between the electrons and the interaction between the donor impurity ions, respectively. Here, I apply Born-Oppenheimer approximation and the fourth term becomes constant in each realization of the random positions of impurity ions.

15

2.2 Kohn-Sham equations and local density approximation

2.2.1 Density functional theory

Eq. (2.8) is difficult to solve due to the random potential term and electron-electron interaction term. To take into account the Coulomb interaction between electrons, I use density functional theory [37] in this study. The density functional theory consists of two Hohenberg-Kohn's theorem [39, 37], (i) uniqueness theorem and (ii) variational principle with respect to a density.

Uniqueness theorem

A external potential can be uniquely determined by the ground state density in a many-body system except for a constant, i.e. the Hamiltonian and, therefore, any physical quantities are also determined uniquely by the ground state density.

Variational principle

There exists an energy functional for a given external potential. For the external potential, the exact ground state energy of the system is the global minimum value of this functional, and the density that minimizes the functional is the exact ground state density.

From uniqueness theorem one can define a ground state energy functional with respect to a density.

$$E_g = E_g\left[n\right] \equiv F_{\mathrm{HK}}\left[n\right] + \int d^3r\, V_{\mathrm{ext}}\left[n\right]\left(\boldsymbol{r}\right) n\left(\boldsymbol{r}\right) \qquad (2.9)$$

where $n(\boldsymbol{r})$ is a density and $V_{\mathrm{ext}}\left[n\right]$ is a external potential. The universal functional F_{HK} is defined as

$$F_{\mathrm{HK}}\left[n\right] \equiv \langle \Psi\left[n\right]| \left(\hat{T} + \hat{V}_{\mathrm{int}}\right) |\Psi\left[n\right]\rangle \qquad (2.10)$$

$\Psi\left[n\right]$ is a ground state wavefunction of $V_{\mathrm{ext}}\left[n\right]$. $\hat{T}$ is an operator for the kinetic energy and V_{int} is an interaction energy between electrons. In Eq. (2.9) the external potential also varies such that the density becomes the ground state

16

density in the external potential. And I consider other functional defined by

$$E_V[n] \equiv \langle \Psi[n]| \hat{T} + \hat{V}_{\text{int}} + \hat{V} |\Psi[n]\rangle \tag{2.11}$$

$$= F_{\text{HK}}[n] + \int d^3r \, V(\boldsymbol{r}) \, n(\boldsymbol{r})$$

with given external potential V. Eq. (2.11) can be defined for any density which has a corresponding V_{ext}. Note that V does not depend on the density n. Eq. (2.11) shows the minimum value when n is equivalent to the ground state density n_0 of the external potential V.

$$E_V[n] \geq E_V[n_0] \tag{2.12}$$

2.2.2 Kohn-Sham equations

In this section, I derive Kohn-Sham equation [40] using the density functional theory. The Kohn-Sham equations are similar to the Schrödinger equation but it is for an auxiliary non-interacting system. By using Hohenberg-Kohn's theorems, finding a ground state with given external potential is achieved by minimizing the energy functional Eq. (2.11) with respect to the density, instead of a many-body wavefunction. Then, I assume there exists the auxiliary non-interacting system in which the ground state density is equal to the true ground state density of the original many-body system. One can define the ground state in the auxiliary system.

$$\Phi_{\text{KS}} \equiv \frac{1}{\sqrt{N!}} \det\left(\{\phi_i(\boldsymbol{r}_j)\}_{i,j=1 \; N}\right) \tag{2.13}$$

The density is derived using $\{\phi_i\}$

$$n(\boldsymbol{r}) = N \int d^3r_2 \cdots d^3r_N \, |\Phi_{KS}(\boldsymbol{r}, \boldsymbol{r}_2, \cdots, \boldsymbol{r}_N)|^2 \tag{2.14}$$

$$= \sum_i |\phi_i(\boldsymbol{r})|^2 \tag{2.15}$$

Before taking variation, I separate Eq. (2.10) as

$$F_{\text{HK}}[n] = T_s[n] + E_{\text{Hartree}}[n] + E_{\text{XC}}[n] \tag{2.16}$$

where

$$T_s\left[n\right] \equiv -\frac{1}{2}\sum_i^N \langle\phi_i|\nabla^2|\phi_i\rangle \qquad (2.17)$$

$$E_{\text{Hartree}}\left[n\right] \equiv \frac{1}{2}\iint d^3r\, d^3r'\, \frac{n\left(\bm{r}\right)n\left(\bm{r}'\right)}{|\bm{r}-\bm{r}'|} \qquad (2.18)$$

$$E_{\text{XC}}\left[n\right] \equiv F_{\text{HK}}\left[n\right] - T_s\left[n\right] - E_{\text{Hartree}}\left[n\right] \qquad (2.19)$$

Eqs. (2.17), (2.18), and (2.19) are universal functionals of the density. Then, I consider variational problem for Eq. (2.11) with respect to the auxiliary orbitals. Note that the orbitals satisfy normalization constraint.

$$\frac{\delta}{\delta\phi_i^*}\left(E_V\left[n\right] - \sum_i \epsilon_i\left(1 - \int d^3r\,\left|\phi_i\left(\bm{r}\right)\right|^2\right)\right) = 0 \qquad (2.20)$$

From Eq. (2.20), I obtain Kohn-Sham equations below.

$$\left(-\frac{1}{2}\nabla^2 + V_{\text{eff}}\left[n\right]\right)\phi_i\left(\bm{r}\right) = \epsilon_i\phi_i\left(\bm{r}\right) \quad (i = 1,\ldots,N) \qquad (2.21)$$

$$V_{\text{eff}}\left[n\right] = V_{\text{ext}} + V_{\text{Hartree}}\left[n\right] + V_{\text{XC}}\left[n\right] \qquad (2.22)$$

where

$$V_{\text{Hartree}}\left[n\right] \equiv \int d^3r'\,\frac{n\left(\bm{r}'\right)}{|\bm{r}-\bm{r}'|} \qquad (2.23)$$

and

$$V_{\text{XC}}\left[n\right] \equiv \frac{\delta E_{\text{XC}}\left[n\right]}{\delta n} \qquad (2.24)$$

The total energy can be expressed as,

$$E_{\text{total}} \equiv T_s + E_{\text{ext}} + E_{\text{Hartree}} + E_{\text{XC}} + E_{\text{II}} \qquad (2.25)$$

$$= \sum_i^N \epsilon_i - \frac{1}{2}E_{\text{Hartree}} - \int d^3r\, V_{\text{XC}}\left(\bm{r}\right)n\left(\bm{r}\right) + E_{\text{XC}} + E_{\text{II}} \quad (2.26)$$

where E_{II} is a energy between nuclei. While in principle the Kohn-Sham equations are exact, in practice the exact form of the exchange-correlation energy is not known and an approximation is required. This scheme can be generalized to a spin polarized case [39].

18

2.2.3 Local density approximation

The exact ground state density and energy are obtained by solving the Kohn-Sham equations if one knows the exact form of the exchange-correlation energy. However, the functional form is not known and I use the local density approximation [39] in this work. In local density approximation, the exchange-correlation energy functional is approximated as

$$E_{\text{XC}} \simeq E_{\text{XC}}^{\text{LDA}} \equiv \int d^3r \; \epsilon_{\text{XC}} \left(n\left(\boldsymbol{r}\right), \zeta\left(\boldsymbol{r}\right)\right) n\left(\boldsymbol{r}\right) \qquad (2.27)$$

where total charge density, $n(\boldsymbol{r})$, and spin density, $\zeta(\boldsymbol{r})$, are defined using up- and down-spin density, $n^\uparrow$ and $n^\downarrow$ as,

$$n \equiv n^\uparrow + n^\downarrow \qquad (2.28)$$

$$\zeta \equiv \frac{n^\uparrow - n^\downarrow}{n} \qquad (2.29)$$

I use the form of ϵ_{XC} given in Eq. (2) of Ref. [44] though with the parameter values given in Ref. [45] rather than Ref. [44]. ϵ_{XC} is separated into an exchange part ϵ_{X} and correlation part ϵ_{C}. Spin dependence of ϵ_{X} and ϵ_{C} is described using $f\left(\zeta\right)$ as

$$\epsilon_{\text{X,C}}\left(n, \zeta\right) = \epsilon_{\text{X,C}}^{P}\left(n\right) + \left[\epsilon_{\text{X,C}}^{F}\left(n\right) - \epsilon_{\text{X,C}}^{P}\left(n\right)\right] f\left(\zeta\right) \qquad (2.30)$$

$$f\left(\zeta\right) \equiv \frac{\left(1+\zeta\right)^{4/3} + \left(1-\zeta\right)^{4/3} - 2}{2\left(2^{1/3} - 1\right)} \qquad (2.31)$$

where superscript ^{P} and ^{F} mean paramagnetic and ferromagnetic configurations. Each energy density in Eq. (2.30) is given as

$$\epsilon_{\text{X}}^{P} = -\frac{3}{4}\left(\frac{3}{\pi}\right)^{1/3} n^{1/3} \qquad (2.32)$$

$$\epsilon_{\text{X}}^{F} = -\frac{3}{4}\left(\frac{6}{\pi}\right)^{1/3} n^{1/3} \qquad (2.33)$$

$$\epsilon_{\text{C}}^{P} = -c^{P}\left[\left(1 + \left(\frac{r_s}{r^P}\right)^3\right) \ln\left(1 + \frac{r^P}{r_s}\right) + \frac{1}{2}\frac{r_s}{r^P} - \left(\frac{r_s}{r^P}\right)^2 - \frac{1}{3}\right] \qquad (2.34)$$

$$\epsilon_{\text{C}}^{F} = -c^{F}\left[\left(1 + \left(\frac{r_s}{r^F}\right)^3\right) \ln\left(1 + \frac{r^F}{r_s}\right) + \frac{1}{2}\frac{r_s}{r^F} - \left(\frac{r_s}{r^F}\right)^2 - \frac{1}{3}\right] \qquad (2.35)$$

where r_s is defined as

$$r_s \equiv \left(\frac{3}{4\pi}\right)^{1/3} n^{-1/3} \qquad (2.36)$$

c^P, c^F, r^P, and r^F are fitting parameters shown in Table 2.1. c^P and c^F have an energy unit and r^P and r^F have a length unit. The values shown in the table are described in the Hartree atomic units in a free space. (I apply these parameters to the effective medium in Sec. 2.2.4.)

Table 2.1: The values of fitting parameter for the exchange-correlation functional given in Ref. [45].

c^P	0.0225		r^P	21.0
c^F	$\dfrac{0.0225}{2^{1/3}}$		r^F	$21.0 \times 2^{1/3}$

It is convenient to define the exchange and correlation potentials for paramagnetic and ferromagnetic systems.

$$V_X^P = -\left(\frac{3}{\pi}\right)^{1/3} n^{1/3} \qquad (2.37)$$

$$V_X^F = -\left(\frac{6}{\pi}\right)^{1/3} n^{1/3} \qquad (2.38)$$

$$V_C^P = -c^P \ln\left(1 + \frac{r^P}{r_s}\right) \qquad (2.39)$$

$$V_C^F = -c^F \ln\left(1 + \frac{r^F}{r_s}\right) \qquad (2.40)$$

From Eq. (2.24) and Eq. (2.27) one can derive the spin dependent exchange-correlation potential.

$$
\begin{aligned}
V_{X,C}^{\uparrow,\downarrow} &= \frac{\delta n}{\delta n^{\uparrow,\downarrow}} \frac{\delta E_{XC}^{LDA}[n,\zeta]}{\delta n} + \frac{\delta \zeta}{\delta n^{\uparrow,\downarrow}} \frac{\delta E_{XC}^{LDA}[n,\zeta]}{\delta \zeta} \\
&= V_{X,C}^P(n) + \left(V_{X,C}^F(n) - V_{X,C}^P(n)\right) \cdot f(\zeta) \\
&\quad \pm \left(\epsilon_{X,C}^F(n) - \epsilon_{X,C}^P(n)\right) \cdot (1 \mp \zeta) \frac{\delta f(\zeta)}{\delta \zeta} \qquad (2.41)
\end{aligned}
$$

20

2.2.4 Kohn-Sham equations within an effective medium

In the literature the density functional theory and Kohn-Sham equations are considered for electrons in free space whereas I need a scheme for an effective medium. I have to give the functional form for the exchange-correlation energy in an effective medium. To map the expressions for the exchange-correlation energy in free space to the formulae I require here, I re-scale lengths and energies according to the formulae

$$\tilde{\boldsymbol{r}} = \left(\frac{m_e^*}{\varepsilon_r}\right) \boldsymbol{r} \;, \quad \tilde{E} = \left(\frac{\varepsilon_r^2}{m_e^*}\right) E \qquad (2.42)$$

The units of lengths and energies having tilde are replaced as [Bohr] $\rightarrow$ [(ε_r/m_e^*)Bohr] and [Hartree] $\rightarrow$ [(m_e^*/ε_r^2)Hartree], respectively. In this section symbols having tilde are described in this new units. After this re-scaling the effective mass and dielectric constant vanish in the Hamiltonian of Eq. (2.8). Then, I apply the density functional theory and Kohn-Sham equations to the new Hamiltonian which does not contain the effective mass and dielectric constant. Note that normalization condition affects the density by this re-scaling and density described in the new units relates with the density in the atomic units as

$$\tilde{n}\left(\tilde{\boldsymbol{r}}\right) = \left(\frac{\varepsilon_r}{m_e^*}\right)^3 n\left(\boldsymbol{r}\right) \qquad (2.43)$$

Energy functionals within the atomic units relate with those within the new units as

$$E\left[n\right] = \frac{m_e^*}{\varepsilon_r^2} \cdot \tilde{E}\left[\tilde{n}\right] \qquad (2.44)$$

From Eq. (2.44) one obtains the Kohn-Sham equations with the effective mass and dielectric constant.

$$\left(-\frac{1}{2m_e^*}\nabla^2 + V_{\text{eff}}\left[n\right]\right)\phi_i\left(\boldsymbol{r}\right) = \epsilon_i\phi_i\left(\boldsymbol{r}\right) \quad (i = 1, \ldots, N) \qquad (2.45)$$

$$V_{\text{eff}}\left[n\right] = -\frac{1}{\varepsilon_r}\sum_{I=1}^{N}\frac{1}{|\boldsymbol{r}-\boldsymbol{R}_I|} + \frac{1}{\varepsilon_r}\int d^3r'\,\frac{n\left(\boldsymbol{r}'\right)}{|\boldsymbol{r}-\boldsymbol{r}'|} + V_{\text{XC}}\left[n\right] \qquad (2.46)$$

where

$$V_{\text{XC}}\left[n\right]\left(\boldsymbol{r}\right) = \frac{m_e^*}{\varepsilon_r^2} \cdot \tilde{V}_{\text{XC}}\left[\tilde{n}\right]\left(\tilde{\boldsymbol{r}}\right) \qquad (2.47)$$

The expression of $\tilde{V}_{\text{XC}}$ is the formulae given in free space.

In this study I apply local density approximation for the exchange-correlation energy. Due to this re-scaling the units of the parameters shown in Table 2.1 are replaced by $[(\varepsilon_r/m_e^*)\text{Bohr}]$ and $[(m_e^*/\varepsilon_r^2)\text{Hartree}]$, respectively.

2.3 Multi-fractal finite size scaling

2.3.1 Multi-fractal exponents as a measure of the localization

To evaluate the metal-insulator transition from the ground state calculation I use a technique based on multi-fractal analysis [16, 17]. In this study I calculate multi-fractal exponents as a measure of localization. Suppose a system with linear size L is separated into small boxes which have linear size l as shown in Fig. 2.2. One can define a coarse grained intensity, $\{\mu_k\}$.
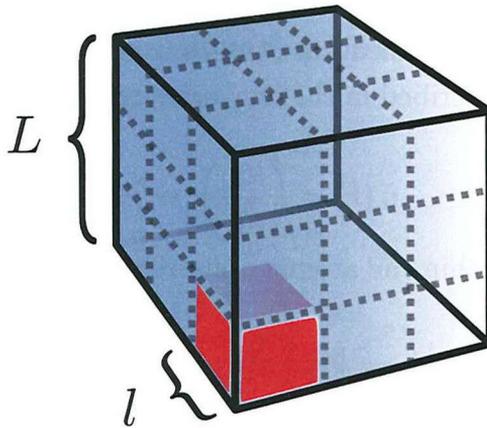
Figure 2.2: This figure shows coarse graining of a system. L and l mean the linear size of the system and coarse grained boxes, respectively.

$$\mu_k \equiv \int_{k\text{th box}} d^3r \, |\phi(\boldsymbol{r})|^2 \qquad (2.48)$$

where the integration is done for each coarse grained box and subscript, k, indicates the index of coarse grained boxes. In this study the integrand of

Eq. (2.48) is the highest occupied Kohn-Sham orbitals obtained from the self-consistent calculation for Eqs. (2.45) and (2.46). By using $\{\mu_k\}$ a generalized inverse participation ratio is defined as

$$R_q \equiv \sum_k (\mu_k)^q \qquad (2.49)$$

and its differentiation with respect to the exponent, q, as

$$S_q \equiv \sum_k (\mu_k)^q \ln \mu_k \qquad (2.50)$$

One can define the multi-fractal exponents, $\tilde{\tau}_q$ and $\tilde{\alpha}_q$, from Eqs. (2.49) and (2.50).

$$\tilde{\tau}_q \equiv \frac{\ln \langle R_q \rangle}{\ln \lambda} \qquad (2.51)$$

$$\tilde{\alpha}_q \equiv \frac{\langle S_q \rangle}{\langle R_q \rangle \ln \lambda} \qquad (2.52)$$

Here λ is defined as a ratio between l and L.

$$\lambda \equiv \frac{l}{L} \qquad (2.53)$$

The errors for multi-fractal exponents, $\sigma_{\tilde{\tau}_q}$ and $\sigma_{\tilde{\alpha}_q}$, are estimated as [17],

$$\sigma_{\tilde{\tau}_q} = \frac{\sigma_{\langle R_q \rangle}}{\langle R_q \rangle \ln \lambda} \qquad (2.54)$$

$$\sigma_{\tilde{\alpha}_q} = \frac{1}{\ln \lambda} \sqrt{\frac{\sigma^2_{\langle S_q \rangle}}{\langle R_q \rangle^2} + \frac{\langle S_q \rangle^2 \sigma^2_{\langle R_q \rangle}}{\langle R_q \rangle^4} - \frac{2\langle S_q \rangle}{\langle R_q \rangle^3} \mathrm{cov}\left(\langle S_q \rangle, \langle R_q \rangle\right)} \qquad (2.55)$$

where $\sigma_{\langle R_q \rangle}$ and $\sigma_{\langle S_q \rangle}$ are the error for R_q and S_q, respectively. Note that covariance between R_q and S_q is included in Eq. (2.55).

Note that the Kohn-Sham orbital is not an electronic state in principle. The Kohn-Sham orbital is nothing but an auxiliary state. However, if the correlation effect is small, the shape of Kohn-Sham orbital can be some sort of "zeroth" order perturbation for a quasi-particle state [46] and a highest occupied Kohn-Sham orbital mainly contributes the conductive phenomena.

It is helpful to consider the asymptotic behavior of these multi-fractal exponents. For an extended state one can assume that ϕ is a plane wave. In this case μ_k becomes a constant.

$$\mu_k \to \lambda^d \qquad (2.56)$$

23

where d is the dimension of the system. R_q and S_q become as

$$R_q \rightarrow \lambda^{d(q-1)} \tag{2.57}$$

$$S_q \rightarrow \lambda^{d(q-1)} \ln \lambda^d \tag{2.58}$$

Thus the multi-fractal exponents for an extended state are estimated as

$$\tilde{\tau}_q \rightarrow d(q-1) \tag{2.59}$$

$$\tilde{\alpha}_q \rightarrow d \tag{2.60}$$

On the other hand, in the localized phase a minimum value of μ_k exists.

$$\varepsilon \equiv \min \mu_k \tag{2.61}$$

$\varepsilon \rightarrow 0$ in the limit of localization. R_q and S_q, thus the multi-fractal exponents for $q > 0$, $q = 0$, and $q < 0$ show different behaviors, respectively. For $q > 0$, R_q can be estimated as

$$R_q \rightarrow 1 \tag{2.62}$$

The elements of S_q can be separated into a box which involves almost all, i.e. $\mu_k \approx 1$, and almost empty boxes. A contribution from the box which corresponds to $\mu_k = \varepsilon$ is most important for S_q. One can estimate S_q in the localized phase for $q > 0$ as

$$S_q \propto \lim_{\varepsilon \rightarrow 0} \varepsilon^q \ln \varepsilon = 0 \tag{2.63}$$

The multi-fractal exponents in the localized phase for $q > 0$ are

$$\tilde{\tau}_q \rightarrow 0 \tag{2.64}$$

$$\tilde{\alpha}_q \rightarrow 0 \tag{2.65}$$

For $q = 0$,

$$R_0 \rightarrow \lambda^{-d} \tag{2.66}$$

$$S_0 \rightarrow -\infty \tag{2.67}$$

thus, the multi-fractal exponents for $q = 0$ become as

$$\tilde{\tau}_0 \rightarrow -d \tag{2.68}$$

$$\tilde{\alpha}_0 \rightarrow \infty \tag{2.69}$$

24

For $q < 0$, one can estimate R_q as

$$R_q \propto \lim_{\varepsilon \to 0} \frac{1}{\varepsilon^{|q|}} = \infty \tag{2.70}$$

and S_q as

$$S_q \propto \lim_{\varepsilon \to 0} \frac{1}{\varepsilon^{|q|}} \ln \varepsilon = -\infty \tag{2.71}$$

$\tilde{\tau}_q$ for $q < 0$ is derived as

$$\tilde{\tau}_q \to -\infty \tag{2.72}$$

and $\tilde{\alpha}_q$ for $q < 0$ is derived as

$$\tilde{\alpha}_q \propto \lim_{\varepsilon \to 0} \frac{\varepsilon^q \ln \varepsilon}{\varepsilon^q \ln \lambda} \to \infty \tag{2.73}$$

Table 2.2: The asymptotic behaviors of the multi-fractal exponents.

	Extended	Localized
$\tilde{\tau}_q$	$d(q-1)$	$0 \quad (q > 0)$ $-d \quad (q = 0)$ $-\infty \quad (q < 0)$
$\tilde{\alpha}_q$	d	$0 \quad (q > 0)$ $\infty \quad (q \leq 0)$

2.3.2 Finite size scaling for multi-fractal exponents

At the vicinity of the critical impurity concentration, the multi-fractal exponents can be expressed as a scaling function [17, 12].

$$\Gamma_q = \Gamma_q(n_D, L, l) = \mathcal{F}_q\left(\frac{L}{b}, \varrho(n_r) b^{\frac{1}{\nu}}, \eta(n_r) b^y, \lambda\right) \tag{2.74}$$

where Γ_q means $\tilde{\tau}_q$ or $\tilde{\alpha}_q$. b is a re-scaling factor of renormalization group. ϱ is a relevant scaling variable. To consider the finite size effect, an irrelevant

25

scaling variable, η, is introduced. The scaling variables are functions of a reduced impurity concentration defined as,

$$n_r \equiv \frac{n_D - n_c}{n_c} \tag{2.75}$$

In the thermodynamic limit, the multi-fractal exponents are scale invariant at the metal-insulator transition by their definition. Choosing appropriate b Eq. (2.74) can be rewritten as

$$\Gamma_q\left(n_D, L, l\right) = \mathcal{G}'_q\left(\varrho\left(n_r\right) L^{\frac{1}{\nu}}, \eta\left(n_r\right) L^y, \lambda\right) \tag{2.76}$$

In this study I fix λ as a constant and I consider single-parameter finite size scaling for Γ_q.

$$\Gamma_q\left(n_D, L\right) = \mathcal{G}_q\left(\varrho\left(n_r\right) L^{\frac{1}{\nu}}, \eta\left(n_r\right) L^y\right) \tag{2.77}$$

Since the second argument in Eq. (2.77) must vanish in the limit of $L \to \infty$, y must be a negative value. The correlation length, ξ, is related with a relevant scaling variable, ϱ.

$$\xi = \left|\varrho\left(n_r\right)\right|^{-\nu} \tag{2.78}$$

One should consider non-linearity of ϱ and η. These scaling variables can be expanded by Taylor series with some cutoff.

$$\varrho\left(n_r\right) = \sum_{i=1}^{m_\varrho} a_i n_r^i \tag{2.79}$$

$$\eta\left(n_r\right) = \sum_{i=0}^{m_\eta} b_i n_r^i \tag{2.80}$$

m_ϱ and m_η are a cutoff index of the scaling variables. At the critical point where n_r is equal to zero, ϱ must be also zero because Eq. (2.78) diverges at the transition point. Therefore the expansion for ϱ starts from $i = 1$. The scaling function Eq. (2.77) is expressed as a Taylor expansion of the scaling variables.

$$\mathcal{G}_q\left(X, Y\right) = \sum_{i,j=0}^{m_X, m_Y} G_{q,ij} X^i Y^j \tag{2.81}$$

m_X and m_Y are a cutoff index of the Taylor expansion of scaling function with respect to the relevant and irrelevant variables, respectively. The critical

parameters, n_c, $\{a_i\}$, $\{b_i\}$, ν, y, $\{G_{q,ij}\}$ are calculated using the Levenberg-Marquardt method for non-linear fitting [47]. Suppose $\{(n_{D,i}, \Gamma_{q,i}, \sigma_i)\}$ and $\{C_j\}$ are data sets obtained from the self-consistent calculations and the fitting parameters, respectively. The best fit model is determined from the obtained data set by minimizing χ^2.

$$\chi^2 = \sum_i \left(\frac{\Gamma_{q,i} - \Gamma_q\left(n_{D,i}; \{C_j\}\right)}{\sigma_i} \right)^2 \qquad (2.82)$$

There are some non-linear parameters for the scaling function and the diagonal part of a covariant matrix does not directly mean the error of the parameters. The error of these quantities are estimated by using Monte Carlo method [47]. Random sample data sets are generated using the error for each data points. One can apply the same fitting procedure for these generated random data sets and distribution of each quantity is obtained. From the distribution of these quantities, the confidence intervals can be estimated.

2.4 Details of numerical calculations

In this study periodic boundary conditions are imposed. The simulations are performed by generating an ensemble of cubic samples with linear dimension L. The volume of the system is L^3 and the donor concentration is $n_D = N/L^3$. Since I have in mind silicon as the host semiconductor I set

$$m_e^* = 0.32 \ , \ \varepsilon_r = 12.0 \qquad (2.83)$$

The procedure for numerical calculations can be separated into two parts, self-consistent electronic structure calculation (only for electrons in the effective medium) and estimation of the localization and the metal-insulator transition using multi-fractal finite size scaling.

The actual procedure of the former part is described below.

1. The positions of N impurity ions are determined randomly on a simple cubic lattice with lattice constant a_l. This prevents impurity ions being positioned unphysically close together by chance.

2. For numerical purposes the continuous description above is replaced by a discrete description on a real-space grid with spacing a. Laplacian is replaced by using second order finite difference approximations (see Appendix C). The resulting matrices and vectors have dimension equal to the number of grid points $(L/a)^3$. Off-diagonal elements of the Hamiltonian matrices are generated in this step.

3. The potential due to the positive donor impurity ions is calculated by expressing the charge density of the impurity ions as a Fourier series. A cut-off is imposed on the wavenumbers so that the number of terms in this series is equal to the number of the real-space grid. In effect, this replaces the delta-functions of the charge density of the impurity ions with an approximate smooth charge density. Poisson's equation is solved exactly for this approximate density and the corresponding potential obtained using inverse Fourier transform (see Appendix D). This calculation need only be performed once for a given configuration of the impurity ions.

4. The energy between impurity ions is calculated using Ewald sum method [26]. This calculation is also performed once for a given configuration of impurity ions.

5. An initial density is given.

6. The Hartree like term in Eq. (2.45) is evaluated in a similar way for the impurity ion potential. And the exchange-correlation potential is calculated with the local density approximation. Within the local density approximation the exchange-correlation potential term appears only in the diagonal part of the Hamiltonian matrix in the real space. From these functions Eq. (2.46) is evaluated.

7. The N occupied Kohn-Sham orbitals for lowest Kohn-Sham eigenvalues are evaluated by diagonalizing Eq. (2.45). Within the local density approximation the real space finite difference approximation of the Kohn-Sham equations yields a Hamiltonian that is sparse. These orbitals are found using the JADALIMU sparse matrix library [48].

8. Next density is given by the resulted density and previous density with Chebyshev acceleration method. Deviation of the density from previous one is estimated. If the density is not converged, the procedure goes back to Step 6.

9. T_s, E_{ext}, $E_{Hartree}$, and E_{XC} are calculated with the resulted Kohn-Sham orbitals. The expectation values in T_s are approximated by the expectation of discretized Laplacian which is used in the self-consistent calculation. The integration is replaced by summation over the grids. The ground state energy is obtained from these energies.

After repeating the procedure above for each random sample, I moved onto the procedure for estimation of the metal-insulator transition as following.

1. Highest occupied Kohn-Sham orbital is extracted from a converged sample. Using this orbital, coarse grained intensity is estimated. R_q and S_q are calculated for given q values. $\tilde{\alpha}_q$ and $\tilde{\tau}_q$ are derived using R_q and S_q, Eqs. (2.51) and (2.52).

2. The ensemble average of $\tilde{\alpha}_q$ and $\tilde{\tau}_q$ is taken over samples having same system size and impurity concentration.

3. Least square fit for the scaling function, Eq. (2.77). To avoid ambiguity in the definition of the fitting function, Eq. (2.81), I set the coefficient of all first order terms to unity.

$$G_{q,10} = G_{q,01} = 1 \qquad (2.84)$$

The best fit model and corresponding physically important quantities, for example, the critical exponent, are obtained in this step.

4. The errors of the quantities are estimated from Monte Carlo simulation.

Chapter 3

Result

3.1 Spinless system

First I show results for a restricted case that the all electrons in a system have same spin direction. In this spinless case, the number of iteration for self-consistent calculation is roughly 10 times less than the number of iteration for a case that the spin degree of freedom is taken into account. In the spinless case, the impurity band is fully occupied and there is no upper and lower Hubbard bands. I consider the band merging between the impurity band and conduction band in the spinless case instead of between the upper and lower Hubbard bands.

Non-magnetic case leads to unphysical results in low impurity concentration regime. The spin density is fixed to zero in this case and an electron has to share its place with an opposite spin electron. This is unphysical situation and I omitted the analysis for this non-magnetic case.

For the spinless system, ζ defined in Eq. (2.29) is fixed to unity in whole space. The exchange-correlation energy density given in Eq. (2.30) in the spinless system can be expressed as,

$$\epsilon_X\left(n, \zeta = 1\right) = \epsilon_X^F = -\frac{3}{4}\left(\frac{6}{\pi}\right)^{1/3} n^{1/3} \tag{3.1}$$

$$\epsilon_C\left(n, \zeta = 1\right) = \epsilon_C^F \tag{3.2}$$

$$= -c^F\left[\left(1 + \left(\frac{r_s}{r^F}\right)^3\right)\ln\left(1 + \frac{r^F}{r_s}\right) + \frac{1}{2}\frac{r_s}{r^F} - \left(\frac{r_s}{r^F}\right)^2 - \frac{1}{3}\right]$$

31

and the exchange-correlation potential in Eq. (2.41) can be expressed as,

$$V_X^\uparrow = V_X^F = -\left(\frac{6}{\pi}\right)^{1/3} n^{1/3} \qquad (3.3)$$

$$V_C^\uparrow = V_C^F = -c^F \ln\left(1 + \frac{r^F}{r_s}\right) \qquad (3.4)$$

where $c^F = 0.0225/2^{1/3}$ and $r^F = 21.0 \times 2^{1/3}$.

Since I have in mind silicon as a host medium the effective mass and the dielectric constant are $m_e^* = 0.32$ and $\varepsilon_r = 12.0$, respectively. The effective Bohr radius is $a_B^* = 37.5$ Bohr. I used the second order real space finite difference approximation and the grid spacing $a = 18$ Bohr ($= 0.48 \times a_B^*$). The lattice constant a_l of the randomly occupied impurity lattice is fixed such that $a_l/a = 2$. The range of impurity concentration is from $0.42 \times 10^{18} \text{cm}^{-3}$ to $1.3 \times 10^{18} \text{cm}^{-3}$.

3.1.1 Density of states for periodic and disordered systems

The density of states can not describe the metal-insulator transition in the disordered system because it does not distinguish whether the eigenstate is localized or extended. Moreover the critical behavior is not clearly described from the density of states. However, it is worth to compare with results obtained from a periodic system. I compared when the impurity band for different impurity concentrations merges to the conduction band for both the periodic and disordered systems.

Fig. 3.1 shows the density of states for a system in which impurities are arranged in the form of simple cubic lattice. There is one impurity in the simple cubic unit cell. Here the density of states means a number of Kohn-Sham eigenstates which is found in a range between ϵ and $\epsilon + \delta\epsilon$. The density of states in the periodic system is calculated using kernel polynomial method with Jackson kernel [49]. The size of unit cell is changed with keeping the grid spacing fixed. This changes the impurity concentration. The number of polynomials is tuned such that the ratio between number of grids and polynomials becomes similar as possible. This is to keep the finite size ef-

32

fect of kernel polynomial method among the samples for different impurity concentrations.

In Fig. 3.1 the band gap seems to disappear at around $n_D = 1.59 \times 10^{18}$ cm^{-3}, i.e. the metal-insulator transition occurs around this concentration. If one calculate Eq. (2.1) for the periodic system, $n_c^{\frac{1}{3}} a_B^* = 0.23$. This value is not precise because the band edge can not be rigorous in kernel polynomial method and one can calculate the samples only for discrete impurity concentrations.

The average density of states for disordered system is shown in Fig. 3.2. This is a histogram of Kohn-Sham eigenvalues, but not calculated by kernel polynomial method. The band gap does not exist for whole calculated range of impurity concentration in the disordered system. The energy origin among random samples is fixed and an eigenvalue of the highest occupied state for each sample can fluctuate. This corresponds to that the bottom of conduction band in the host medium is fixed as the energy origin among taking the ensemble average.

Fig. 3.3 shows a comparison of the density of states between in the periodic system and disordered system. The band broadening is significant in the disordered system. In this case the randomness gives the competitive effects that it enhances the band gap closing and that the electronic states are localized.

Below the transition concentration of the periodic systems, in disordered systems the band gap has already closed. Actually, the critical concentration in the disordered systems can be estimated as $n_c \approx 1.1 \times 10^{18}$ cm^{-3}, which is explained in Sec. 3.1.2. However, clear singular behavior can not be observed in Fig. 3.2. Thus, some quantitative evaluation of the metal-insulator transition in the disordered system is necessary.
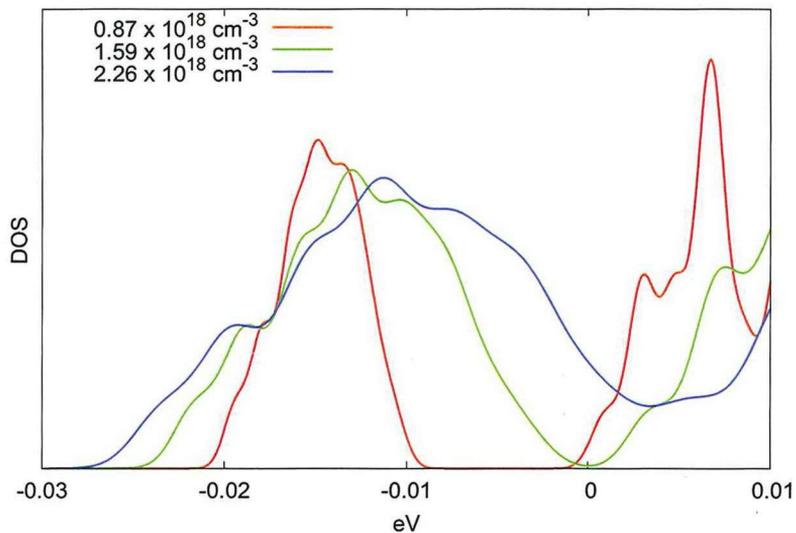
Figure 3.1: The density of states of periodic systems for different impurity concentrations. The number of k-points is 8^3. The size of unit cell is 76.2, 85.7, and 104.8 Å. The number of polynomials is 788, 1122, and 2048, respectively.
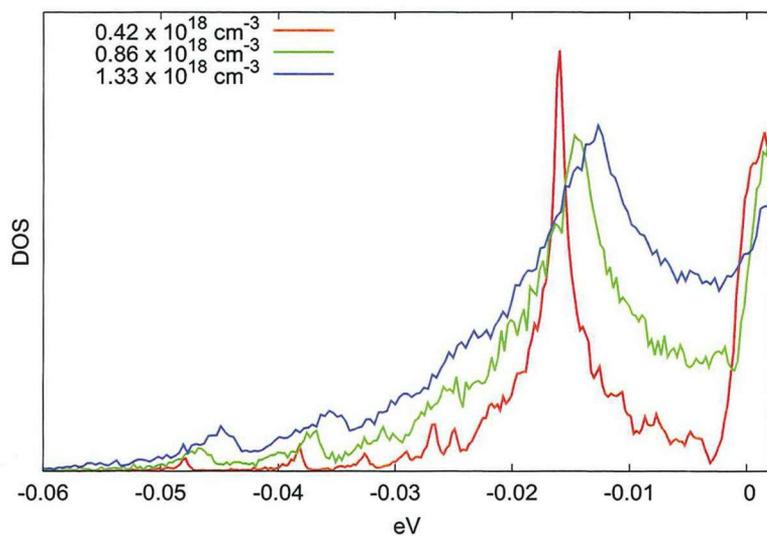
Figure 3.2: The density of states of the disordered system.
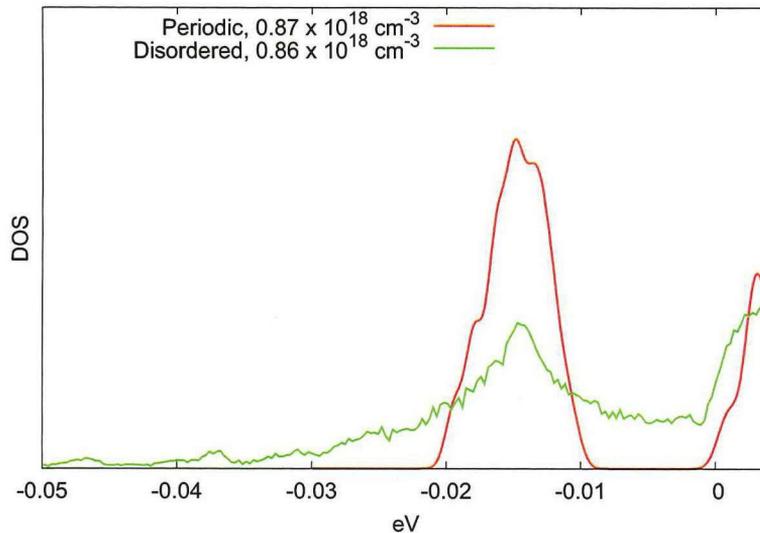
Figure 3.3: The averaged density of states in the disordered system and the density of states in the periodic system. The impurity concentration is about 0.87×10^{18} cm^{-3}.

3.1.2 Results for multi-fractal exponents and finite size scaling

Using the method described in Sec. 2.3, I investigated the critical behavior of the metal-insulator transition in the spinless case. The critical concentration and critical exponent should not depends on q values and the multi-fractal exponents are calculated for some q values to check the consistency. The orbital ϕ in Eq. (2.48) is extracted from self-consistent calculation for Eqs. (2.45) and (2.46). I chose $\lambda = 1/6$ which is defined in Eq. (2.53). The multi-fractal exponents for highest occupied Kohn-Sham orbital as a function of the impurity concentration for different system sizes are shown in Figs. 3.4, 3.5, 3.6, 3.7, 3.8, 3.13, and 3.14. The curves are the best-fit-model obtained by finite size scaling fit. The fitting parameters of scaling function Eq. (2.81) and scaling variables Eqs. (2.79) and (2.80) are determined using, $m_\varrho = 2$, $m_\eta = 1$, $m_X = 3$, $m_Y = 1$. I chose these maximum order of the expansion to avoid unnatural fitting. If one expands the scaling function with higher

35
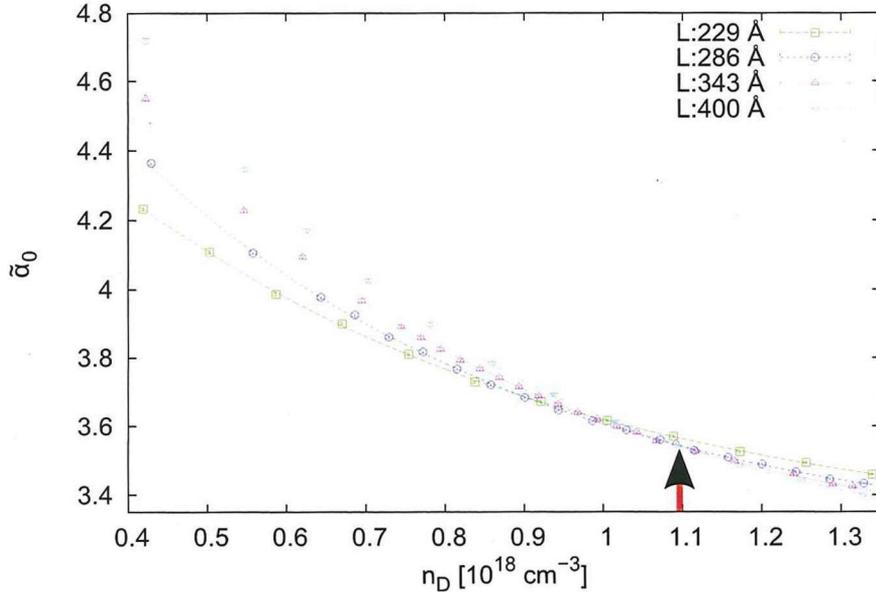
Figure 3.4: $\tilde{\alpha}_0$ for different system sizes as a function of impurity concentration. The number of samples for each data point is between about 1500 to 3000. The critical concentration is indicated by a red arrow.

order, the fitted curves bend unnaturally. On the other hand, the lower order expansion gave the critical concentration out of the calculated range. The number of data points is 67 and the number of fitting parameters is $3 + m_\varrho + (m_\eta + 1) + (m_X + 1) \cdot (m_Y + 1) - 2 = 13$. As described in Sec. 2.3, Eq. (2.77) implies that the distribution of the multi-fractal exponent is scale invariant at the transition provided λ is held fixed. The distribution of $\tilde{\alpha}_0$ shifts to smaller (larger) values in the metallic (localized) phases as the system size increases. For low concentration, typical behavior of localized states is seen, i.e. one can see shifts to larger values as the system size increases. For high concentration the system size dependence is less pronounced but there is a shift to smaller values with increasing system size. (Note there is a lower bound of $\tilde{\alpha}_0 \geq 3$ set by normalization of orbital.)

From the finite size scaling analysis, the critical parameters are obtained. Those obtained for some q values are shown in Table 3.1. The confidence intervals for the critical impurity concentration and critical exponent are determined from the histogram obtained by Monte Carlo simulation. The

36

confidence intervals shown in Table 3.1 are corresponding to 95%. χ^2 values (Eq. (2.82)) and its Q values are also shown in Table 3.1. Q is a probability that an observed χ^2 value accidentally exceeds a given value [47].

Fig. 3.11 shows the histogram for the critical concentrations calculated by Monte Carlo simulation. The critical concentrations agree well between $\tilde{\alpha}_q$ and $\tilde{\tau}_q$ for same q value. However, the critical concentrations of $\tilde{\alpha}_q$ and $\tilde{\tau}_q$ for different q values does not agree with each other. This discrepancy could be caused by irrelevant finite size effect. q value can control weight of ensemble average. For small q, for example, a tail of orbital mainly contributes the mean value. The critical concentration has a tendency of increasing as q is increased. This implies that each contribution of the orbital has different irrelevant finite size effect. Despite of the discrepancy for the critical concentrations, the critical exponents are consistently obtained, $\nu \approx 1.3$, for $\tilde{\alpha}_q$ and $\tilde{\tau}_q$ with some q values.

Note that $\tilde{\alpha}_{0.5}$ has severe property for fitting (Fig. 3.13). The multi-fractal exponents in non-interacting systems follow the symmetry relation [50, 14, 15].

$$\alpha_q + \alpha_{1-q} = 2d \tag{3.5}$$

$\tilde{\alpha}_{0.5}$ in the metallic phase and critical point are both equal to the spatial dimension. Its function of the concentration saturates in the metallic phase and this fact makes the fitting procedure difficult.

The calculation for $q = 1.25$ leads to large confidence intervals for the critical exponents. The large confidence interval can be also seen in Ref. [17]. In addition, the data sets in the present case do not cover vicinity of the crossing point (Fig. 3.14) and the fitting procedure does not work properly.

The order of critical concentration in the present calculation, $n_c \approx 1.1 \times 10^{18} \text{cm}^{-3}$, agrees with the experimental result, $n_c = 3.52 \times 10^{18}$ cm^{-3} [24]. Some of the discrepancy can be explained by the replacement of the semiconductor crystal with an effective medium, i.e. from the universal relationship Eq. (2.1) the predicted critical concentration is 2.25×10^{18} cm^{-3}. The remainder of the discrepancy may result from the following: (i) In the true system spin is not completely polarized. In the system that spin degree of freedom is taken into account, the kinetic energy will be less than the spinless case. Orbital for the spinless case tends to be extended and the hopping integral

can be larger. Thus, the band gap in the spinless system closes earlier than the system that spin is taken into account. (ii) It is known in first principles calculation that the local density approximation underestimates the band gap (see, for example, Ref. [51]). In fact, 1s hydrogen level in the effective medium can be estimated as -0.030 eV, but the peak for low concentration in Fig. 3.1 shows roughly -0.015 eV (even though it is not the isolated atom, one can expect it is close to -0.030 eV for enough large systems).

The critical exponent in the present calculation seems to agrees with one of the experimental value, $\nu(=\mu) = 1.2 \pm 0.2$ [23].

Note that the experimental results for ν ($\nu = \mu$ in 3-dimensional systems [20]) are discussed between ≈ 0.5 (wide region of the concentration) [18, 21] and ≈ 1.0 (narrow region of the concentration) [19, 22] for uncompensated samples. Ref. [23] suggested that $\nu \approx 1.0$ might be attributed by unavoidable compensation in experiment because the critical parameters for compensated samples seem to be similar to the data for uncompensated samples with the narrow range of concentration. However, the scaling analysis basically works more properly as the range of scaling variable becomes narrower. If there exists such narrow region, the analysis within wider region can not be justified. Thus, this agreement can be possible.

The present calculation is for uncompensated spinless systems and these experimental results are for uncompensated systems but the spin direction is not restricted. This difference of the spin degree of freedom can affect the critical parameters.

The non-interacting disordered systems using Anderson model lead to $\nu = 1.590(+0.012, -0.011)$ [17] and it is different from the obtained value in the present work, $\nu \approx 1.3$. If the electron-electron interaction is neglected in this work, it can be equivalent to the topologically disordered systems. The critical exponent calculated in the topologically disordered systems, in which the electron-electron interaction is not taken into account, agrees with the results of the Anderson model, $\nu = 1.61(+0.07, -0.06)$ [25]. The difference from these non-interacting disordered models can be caused by the electron-electron interaction. Because I assumed the electronic correlation is not so strong and it is taken into account only via local density approximation, the long range Coulomb interaction is especially important.
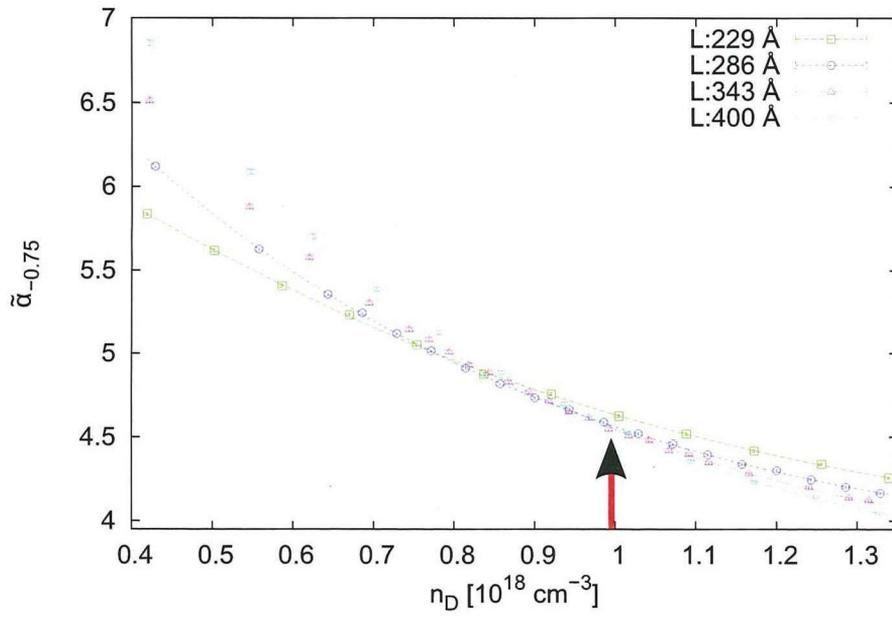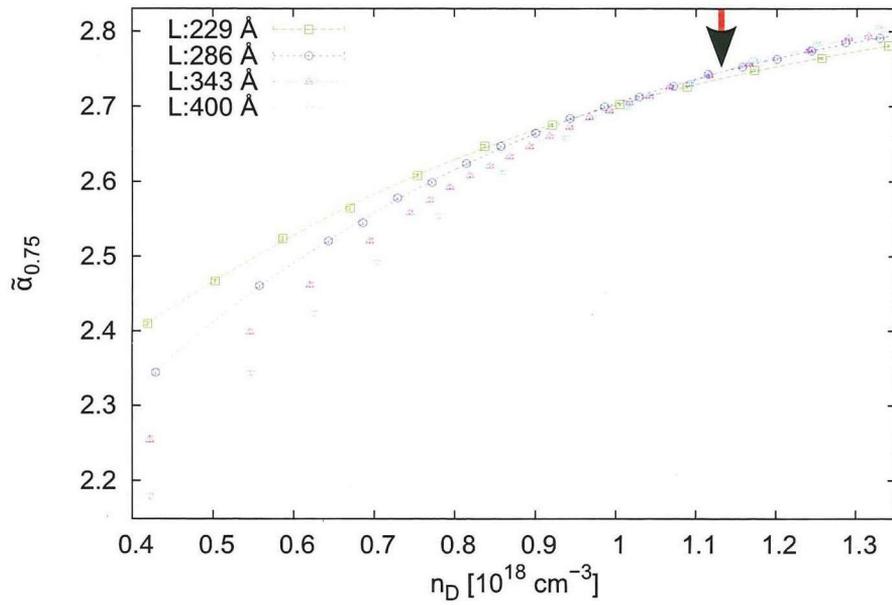
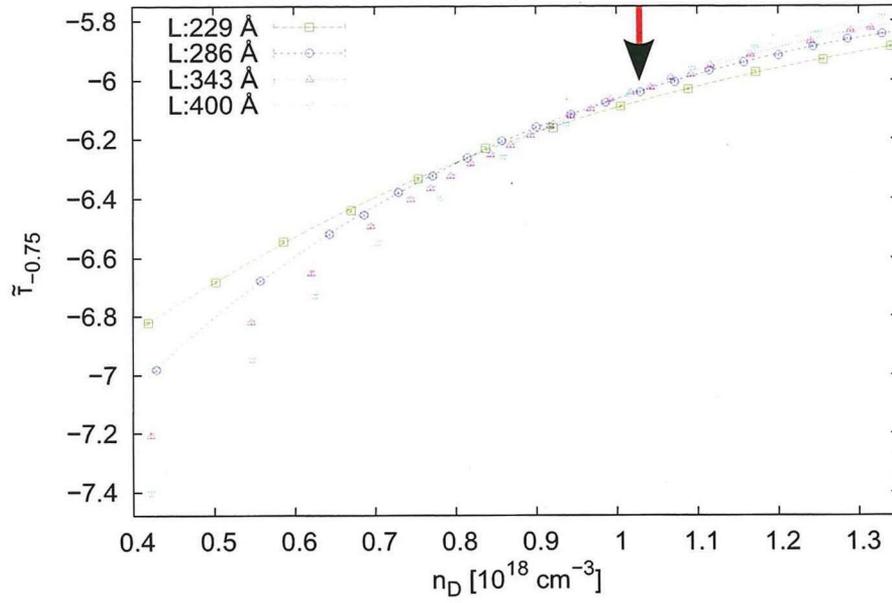Figure 3.5: $\tilde{\alpha}_{-0.75}$.

Figure 3.6: $\tilde{\alpha}_{0.75}$.

39

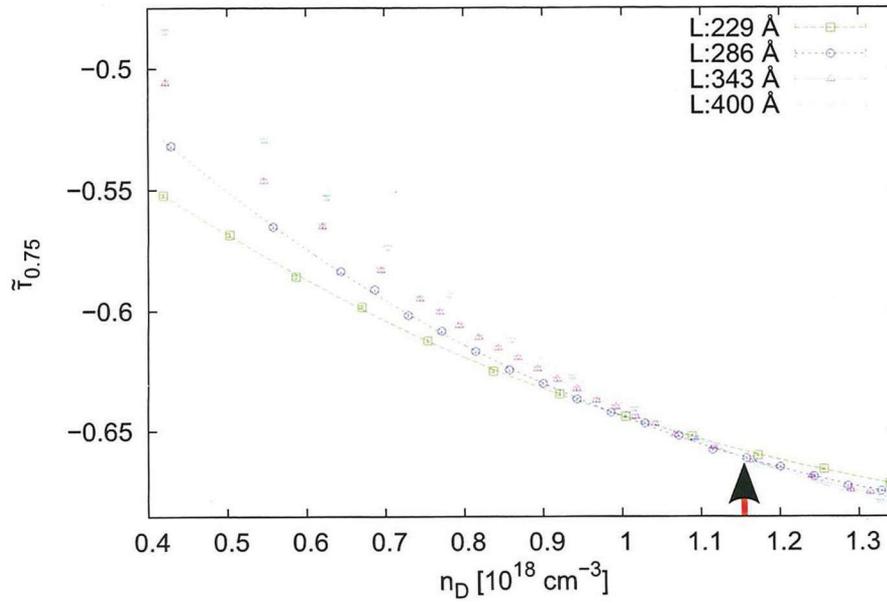Figure 3.7: $\tilde{\tau}_{-0.75}$.

Figure 3.8: $\tilde{\tau}_{0.75}$.

40

Table 3.1: The results for the multi-fractal finite size scaling. The number of data and fitting parameters are 67 and 13, respectively.

	q	ν	$n_c \, [10^{18} \, \mathrm{cm}^{-3}]$	χ^2	Q
$\tilde{\alpha}_q$	-0.75	1.25 (1.19, 1.36)	0.99 (0.96, 1.04)	36.8	0.96
	-0.5	1.29 (1.24, 1.38)	1.02 (0.99, 1.05)	44.3	0.83
	-0.25	1.31 (1.26, 1.40)	1.05 (1.03, 1.09)	52.9	0.49
	0	1.30 (1.24, 1.42)	1.09 (1.08, 1.16)	54.8	0.40
	0.25	1.28 (1.20, 1.43)	1.15 (1.13, 1.19)	48.4	0.70
	0.75	1.28 (1.16, 1.50)	1.13 (1.11, 1.19)	50.2	0.63
	1	1.27 (1.16, 1.46)	1.17 (1.14, 1.23)	47.2	0.77
	1.25	1.48 (1.31, 1.84)	1.19 (1.16, 1.30)	47.0	0.73
$\tilde{\tau}_q$	-0.75	1.29 (1.24, 1.37)	1.03 (1.01, 1.07)	45.2	0.77
	-0.5	1.31 (1.25, 1.39)	1.05 (1.03, 1.09)	51.0	0.59
	-0.25	1.31 (1.25, 1.40)	1.07 (1.05, 1.12)	54.5	0.46
	0.25	1.29 (1.17, 1.43)	1.11 (1.10, 1.17)	52.3	0.47
	0.5	1.29 (1.20, 1.47)	1.14 (1.11, 1.20)	49.4	0.65
	0.75	1.28 (1.20, 1.46)	1.15 (1.13, 1.21)	46.9	0.72
	1.25	1.42 (1.21, 1.63)	1.18 (1.15, 1.23)	47.2	0.73
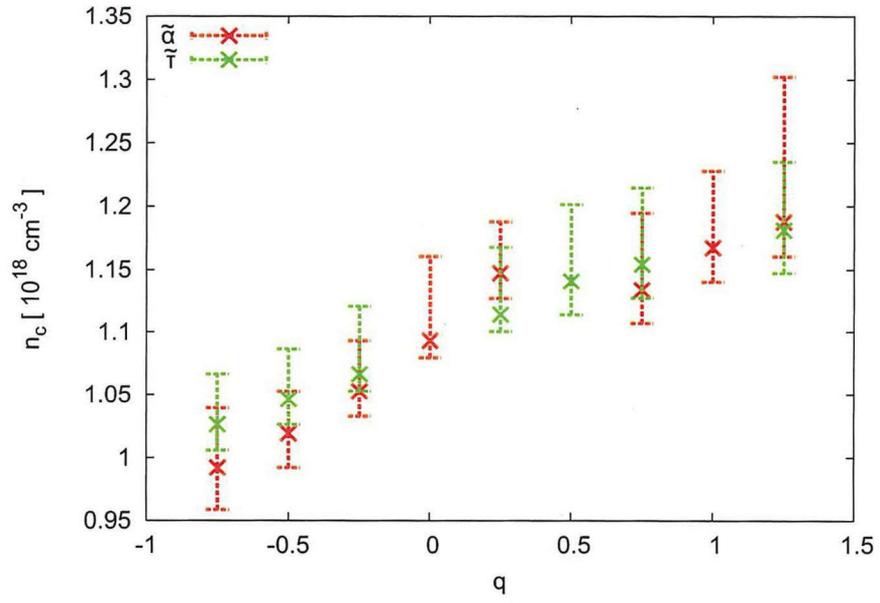
Figure 3.9: n_c as a function of q.
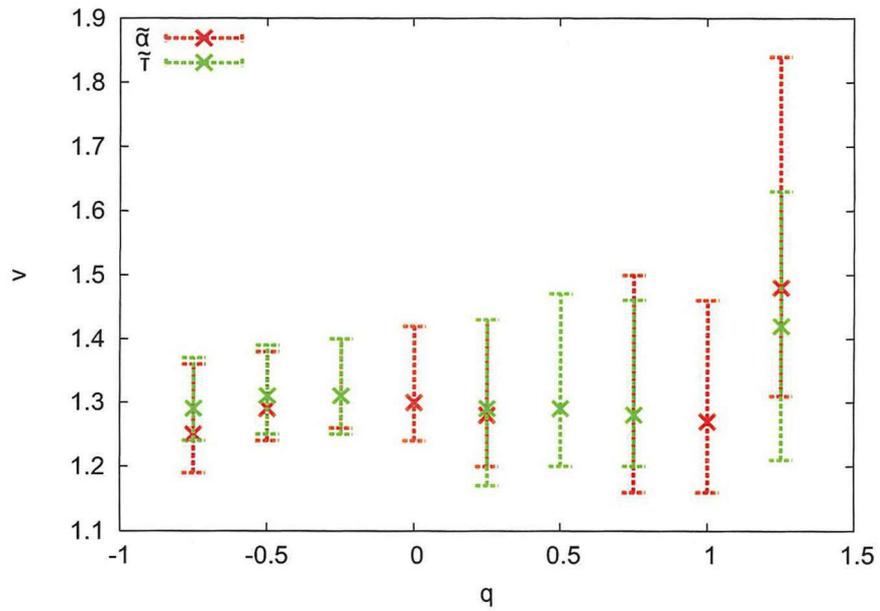
Figure 3.10: ν as a function of q.

42
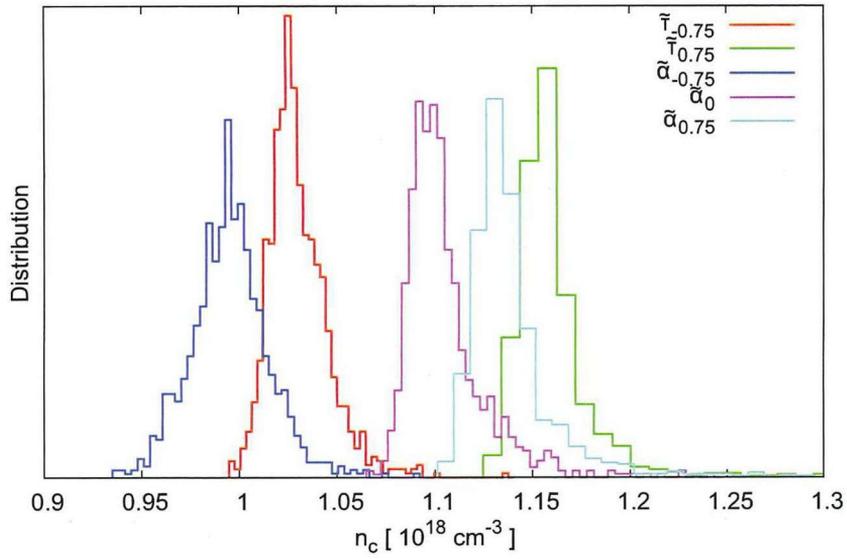
Figure 3.11: Histogram for n_c for different q values obtained by Monte Carlo simulation.
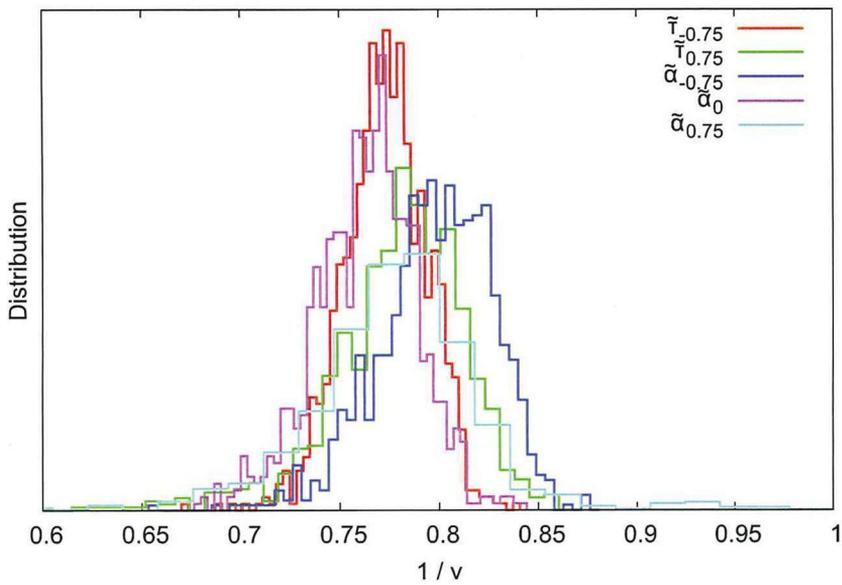
Figure 3.12: Histogram for $1/\nu$ for different q values obtained by Monte Carlo simulation.
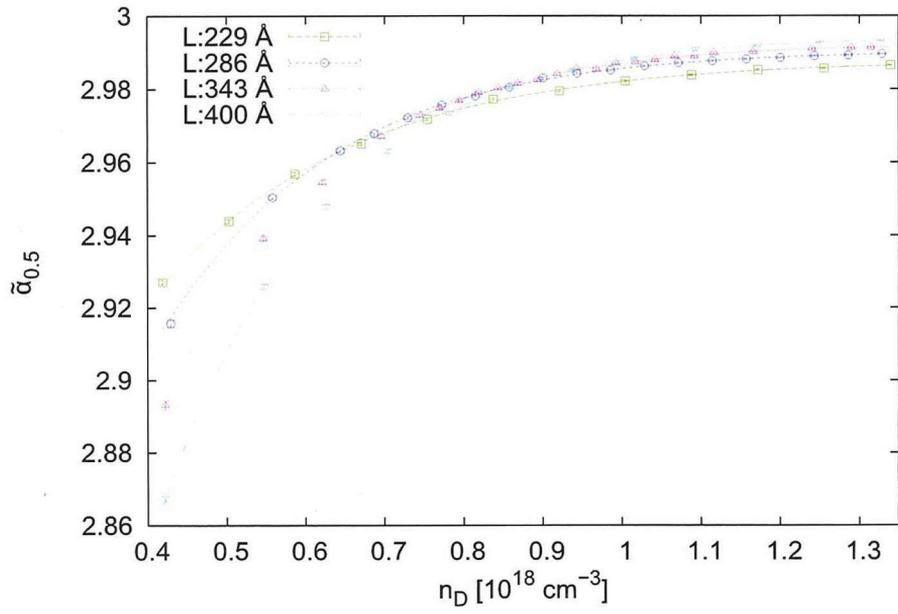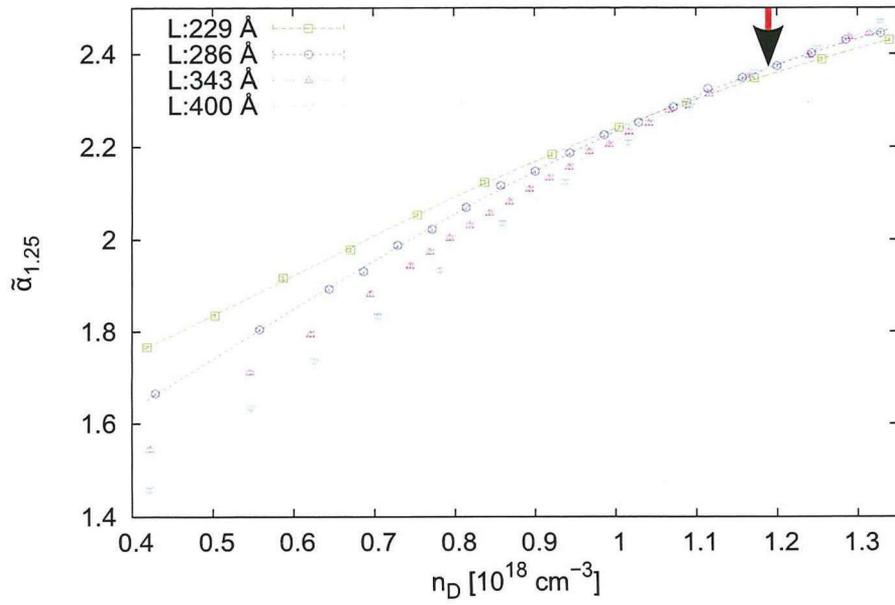
43

Figure 3.13: $\tilde{\alpha}_{0.5}$.

Figure 3.14: $\tilde{\alpha}_{1.25}$.

44

3.1.3   Density for highest occupied Kohn-Sham orbital

To understand more precisely what occurs, here, I show spatial dependence of $|\phi(\boldsymbol{r})|^2$ for the highest occupied Kohn-Sham orbital of typical samples. The system size for Figs. 3.15, 3.16, and 3.17 is $L = 343$ Å. For lower concentration than the critical concentration the Kohn-Sham orbital resembles a molecular orbital on clusters of two or three impurity ions as shown in Fig. 3.15. As the concentration is increased towards the critical concentration the Kohn-Sham orbital spreads out over more impurity ions as shown in Fig. 3.16. For higher concentration than the critical concentration the Kohn-Sham orbital are extended across the entire sample as shown in Fig. 3.17.
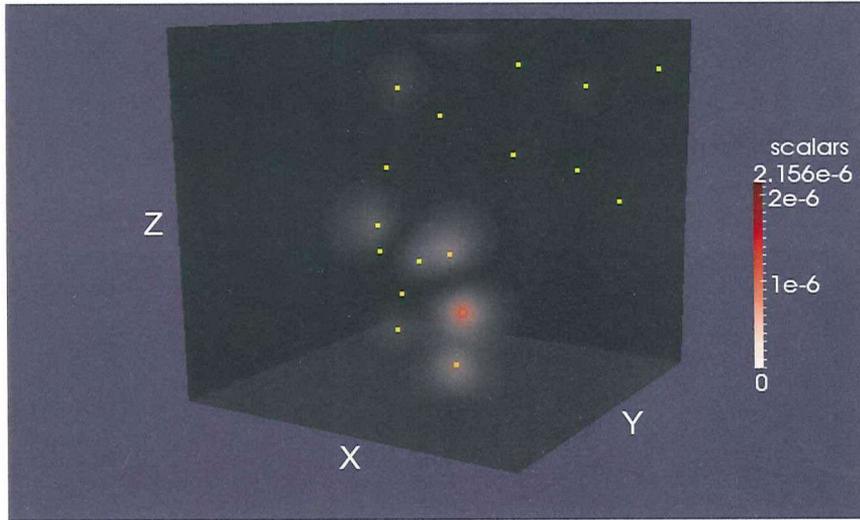
Figure 3.15: Square of highest occupied state, $|\phi(\boldsymbol{r})|^2$, of a sample for $L = 343$ Å and 17 impurities in the spinless system is shown as red cloud. Yellow points are the impurity ions. $n_D = 0.422 \times 10^{18}$ cm^{-3} $(< n_c)$.
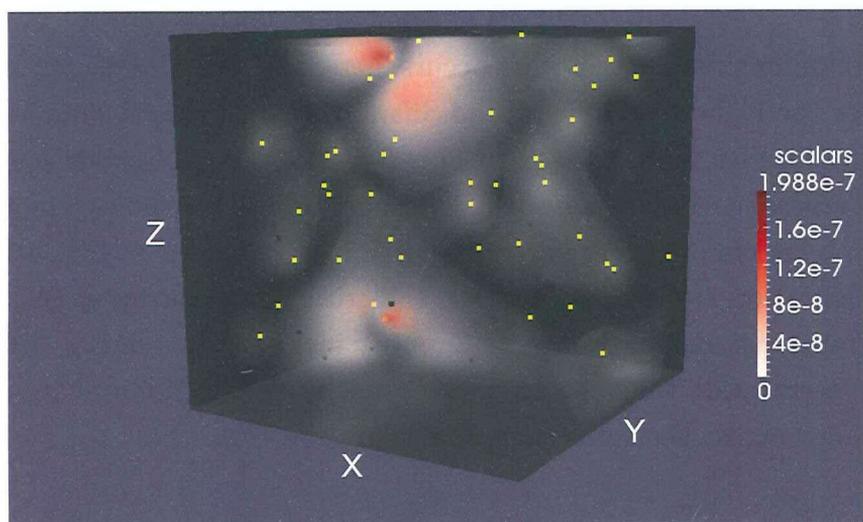
Figure 3.16: The highest occupied state of a sample for $L = 343$ Å and 44 impurities in the spinless system. $n_D = 1.09 \times 10^{18}$ cm^{-3} ($\approx n_c$)
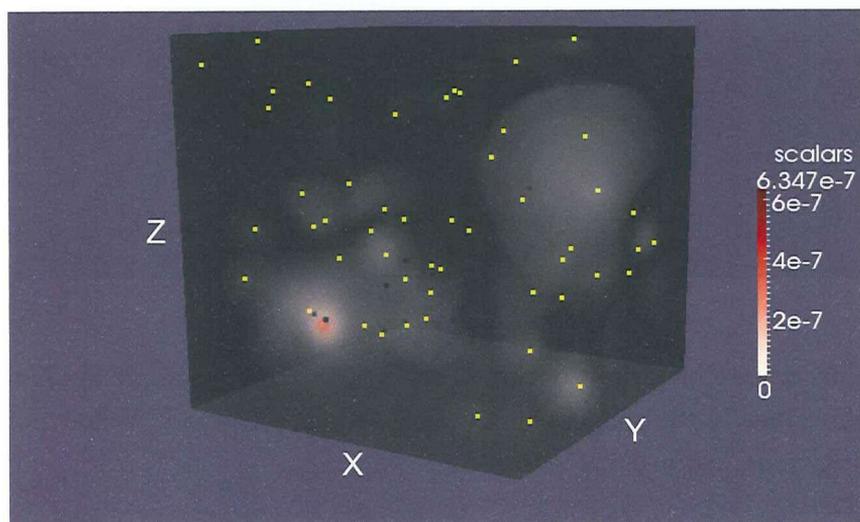

Figure 3.17: The highest occupied state of a sample for $L = 343$ Å and 53 impurities in the spinless system. $n_D = 1.31 \times 10^{18}$ cm^{-3} ($> n_c$).

46

3.2 System with spin

In the previous section I discussed about the spinless case. In this section the restriction for the spin degree of freedom is relaxed. Since I consider an uncompensated system and neglect the multi-valley effect, the system becomes half-filling. For the spinless case, the metal-insulator transition occurs between the impurity band and conduction band. When the restriction is relaxed, half of the impurity band is occupied and the metal-insulator transition occurs between the upper and lower Hubbard bands.
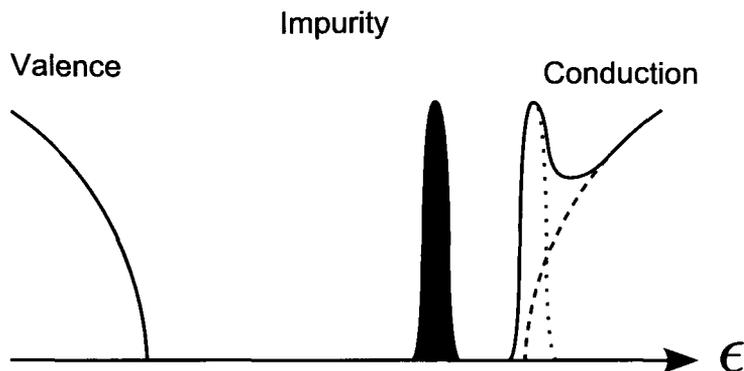
Figure 3.18: The upper and lower Hubbard bands separated from the impurity band. From Ref. [24] the upper Hubbard band can be close to, or already merged to the conduction band.

I report some results for the system. From the results I would like to show some proposals.

3.2.1 Results for multi-fractal exponents

The results of multi-fractal finite size scaling for the case that the spin is taken into account also shows a crossing (Fig. 3.19). The critical concentration can be found around $1.5 \times 10^{18} \text{cm}^{-3}$. This is closer to the experimental value $n_c = 2.25 \times 10^{18} \text{cm}^{-3}$ than that of the spinless systems $n_c \approx 1.1 \times 10^{18} \text{cm}^{-3}$. In the system with spin, the crossing point is more ambiguous than the spinless system. Thus, it is difficult to fit the scaling function. This implies

47

that the irrelevant finite system size effect is large in this case (Eq. (2.80)).

I show two curves for the smallest system, $L = 171$Å, in Fig. 3.19. These curves correspond to the systems including odd and even number of impurities, respectively. The separation is significant especially around low impurity concentration. This separation is not observed around high impurity concentration in the smallest systems and whole range of concentration in the larger systems. This is an irrelevant effect of the finite number of impurities.

From these results, I suggest the calculation must be done with larger system size than $L = 171$Å.
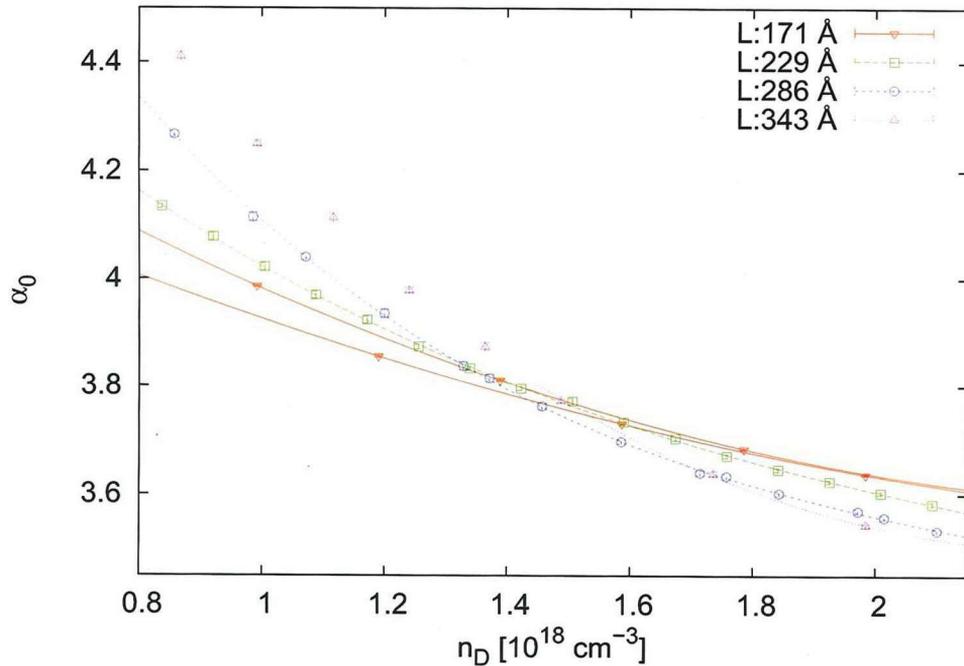

Figure 3.19: A result of $\tilde{\alpha}_0$ in the case that the spin is taken into account. The number of samples is from about 500 to 5000. The data for $L = 171$ Å are separated into cases of odd and even number of impurities.

3.2.2 Density for highest occupied Kohn-Sham orbital and spin density

In Figs. 3.20, 3.21, and 3.22, similar behavior to the spinless system is observed. Figs. 3.24, 3.26, and 3.28 show the corresponding total spin density. It is expected in a periodic system that the anti-ferromagnetic order appears in the insulating limit and the non-magnetic states are observed in the metallic limit. The both behaviors are observed in the disordered systems for wide range of impurity concentration.
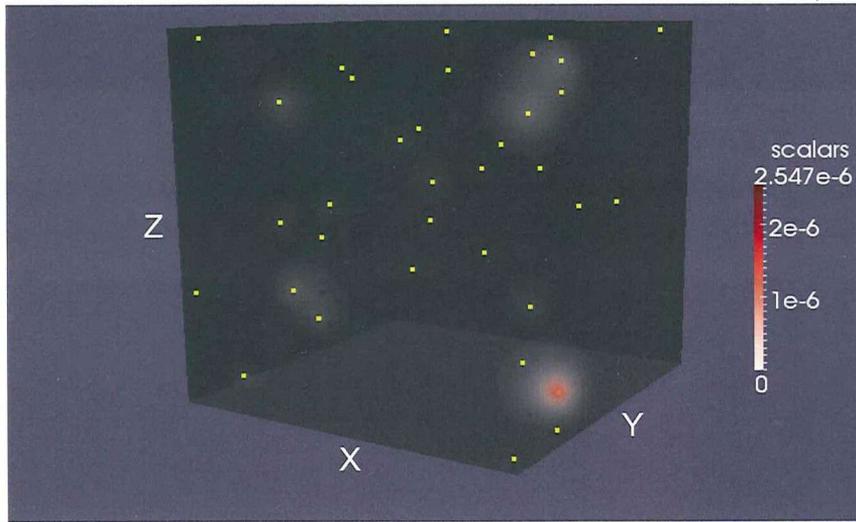

Figure 3.20: Square of highest occupied up-spin state, $|\phi(\boldsymbol{r})|^2$, for $L = 343$ Å and 35 impurities. 19 up-spin and 16 down-spin electrons exist. $n_D = 0.868 \times 10^{18}$ cm^{-3}.
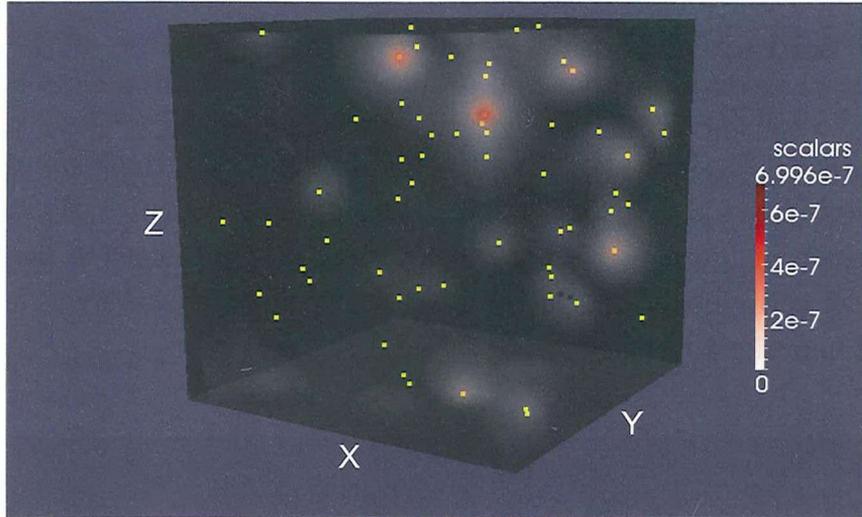
Figure 3.21: The highest occupied up-spin state for $L = 343$ Å, 60 impurities. 30 up-spin and 30 down-spin electrons exist. $n_D = 1.49 \times 10^{18}$ cm^{-3}.
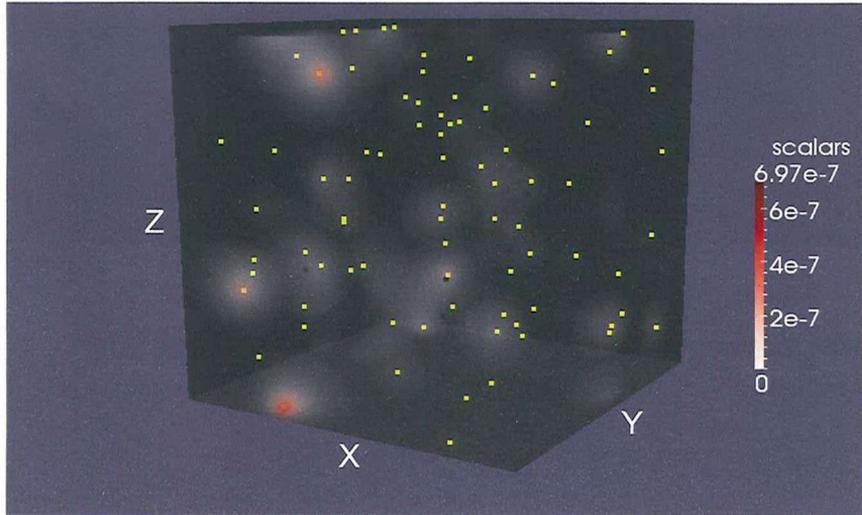

Figure 3.22: The highest occupied up-spin state for $L = 343$ Å, 80 impurities. 41 up-spin and 39 down-spin electrons exist. $n_D = 1.98 \times 10^{18}$ cm^{-3}.
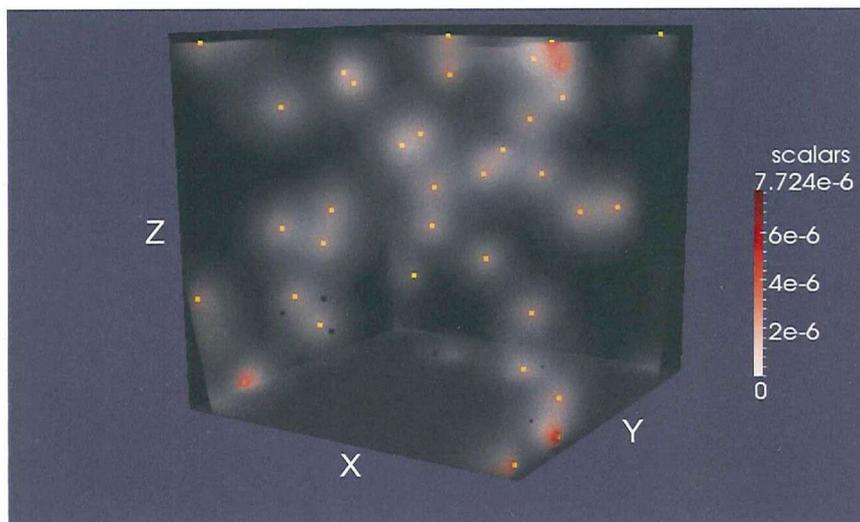
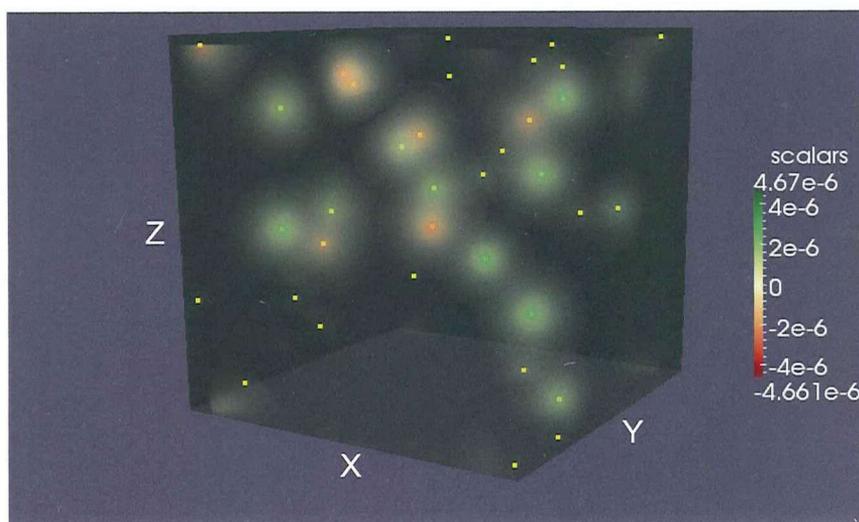Figure 3.23: Total electron density, $n^\uparrow + n^\downarrow$, for $L = 343$ Å and 35 impurities is shown as red cloud.

Figure 3.24: Total spin density, $n^\uparrow - n^\downarrow$, for $L = 343$ Å and 35 impurities is shown as green and red cloud. There exist 19 and 16 up-spin and down-spin electrons, respectively.

51

Figure 3.25: Total electron density for $L = 343$ Å and 60 impurities.

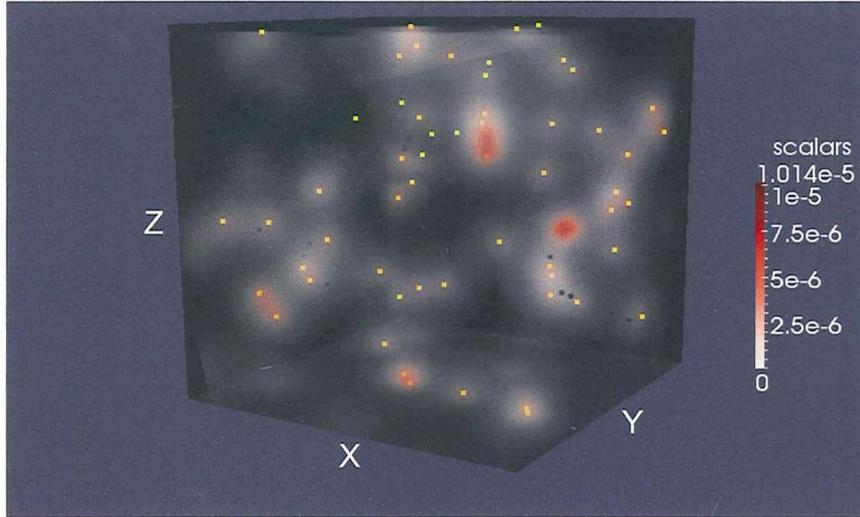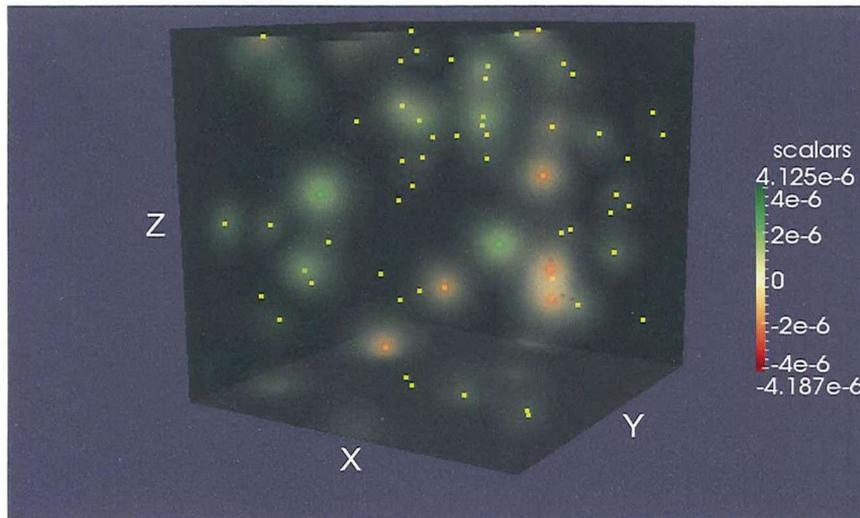Figure 3.26: Total spin density for $L = 343$ Å and 60 impurities. There exist 30 and 30 up-spin and down-spin electrons, respectively.

Figure 3.27: Total electron density for $L = 343$ Å and 80 impurities.

Figure 3.28: Total spin density for $L = 343$ Å and 80 impurities. There exist 41 and 39 up-spin and down-spin electrons, respectively.
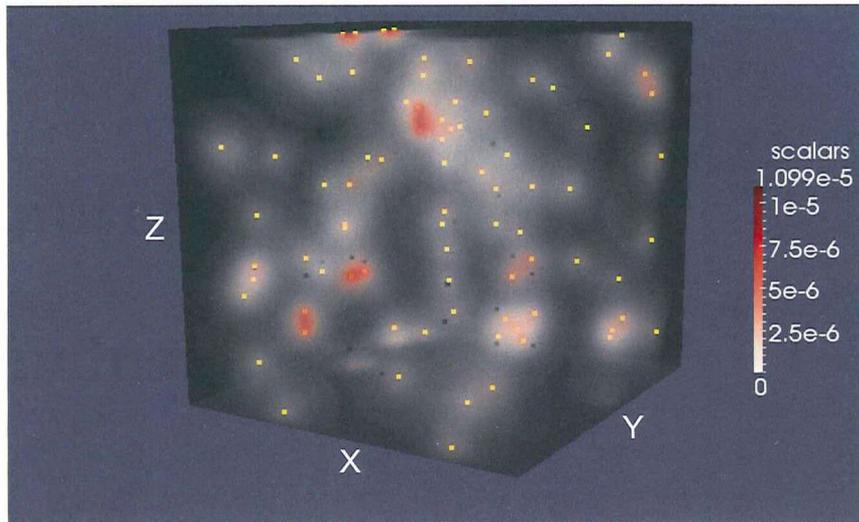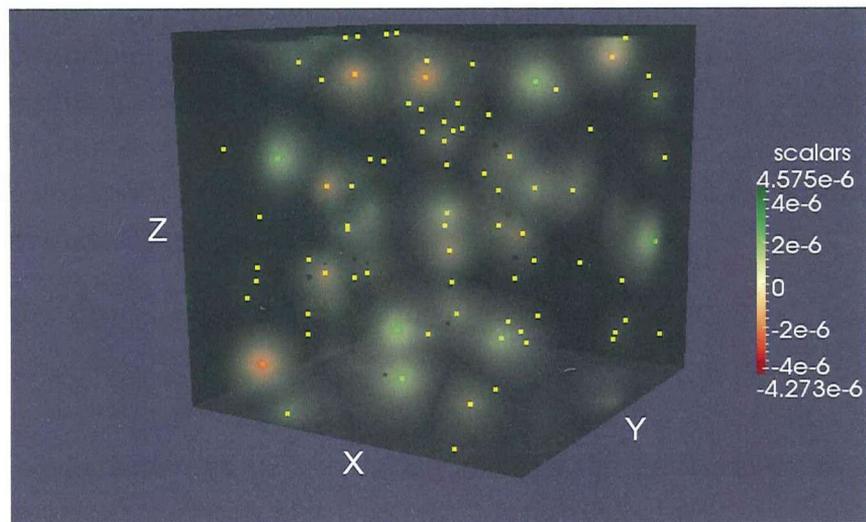
Chapter 4

Conclusion

I simulated the electronic states in the system that impurity ions are randomly distributed and the electrons interact with these impurity ions and with each other via long range Coulomb interaction. I assumed that each impurity supplies one electron. The Hamiltonian in the interacting disordered system is solved by using density functional theory [37, 38, 39] and local density approximation [38, 39] with and without the restriction for the electron spin. For the quantitative analysis of the critical behavior of the metal-insulator transition I applied the multi-fractal finite size scaling [16, 17] to the highest occupied Kohn-Sham orbital.

The important results in the present work are the critical parameters of the metal-insulator transition in the spinless systems.

- The critical exponent of the metal-insulator transition is,

$$\nu = 1.29(+0.08, -0.05) \tag{4.1}$$

  Comparison with the critical exponent of the Anderson transition suggests that the long range Coulomb interaction between electrons changes the universality class of the metal-insulator transition in disordered systems.

- The critical concentration is,

$$n_c \approx 0.992 \sim 1.19 \times 10^{18} \text{ cm}^{-3} \tag{4.2}$$

This range corresponds to,

$$n_c^{\frac{1}{3}} a_B^* \approx 0.20 \sim 0.21 \tag{4.3}$$

These results agree on the order with the experimental results. The physical mechanism of the metal-insulator transition in doped semiconductors can be realized in this model.

Eq. (4.1) is obtained from the result for $\tilde{\tau}_{-0.75}$, which is the most precisely determined with 95% confidence interval. The universality class is distinguished by the critical exponent. Eq. (4.1) is different from the numerical results in the non-interacting systems, 1.57($\pm$0.02) [12], 1.590(+0.012, -0.011) [17], and 1.61(+0.07, -0.06) [25], even though the error is still not enough small. The difference can indicate the long range Coulomb interaction between electrons plays an important role to the critical behavior. To make clearer this suggestion larger number of samples is required to reduce the statistical error and the simulation with larger size systems is necessary to avoid the irrelevant finite size effects.

The critical concentrations in Eq. (4.2) are resulted from the best-fit-models. The order of those critical concentrations agree with the universal relation Eq. (4.4) [27] observed in the experiments with a factor of two.

$$n_c = 2.25 \times 10^{18} \text{ cm}^{-3}$$
$$n_c^{\frac{1}{3}} a_B^* = 0.26 \tag{4.4}$$

The accuracy of those results can be enough to describe the physical mechanisms. The ambiguity of the estimated values for different q values can be resolved by simulating larger systems. The discrepancy between the present work and the experiments in terms of the critical concentration may be improved by better approximations for the exchange-correlation energy functional and relaxing the restriction for the spin degree of freedom. In fact, rough estimate for the system with spin becomes closer to the experimental value than that of the spinless system.

As mentioned in Sec. 2.3.1, the Kohn-Sham orbital is not an physical quantity in principle and the quasi-particle states should be used instead of the Kohn-Sham orbital. This can be done in the perturbative way, as in

GW method [46, 52, 53]. The present results can be a starting point of the method. The calculation will be more time consuming and some efficient methods will be required.

The level curvature with respect to Aharonov-Bohm flux can be a measure of the metal-insulator transition [54, 55]. The highest occupied Kohn-Sham eigenvalue can be related with the ionization energy [56]. The level curvature is a sensitivity of the eigenvalue for the boundary condition.

Similarly, Drude weight [57] can be also a measure of the transition. Drude weight is calculated in the almost same way as the level curvature but the sensitivity of the total energy is used instead of the eigenvalues. This has an advantage that Kohn-Sham scheme can derive the true total energy in principle. Moreover, the another advantage of the Drude weight is that one can exploit local force theorem [58] to reduce calculation cost.

I expect that more interesting things for the metal-insulator transition, not only for the critical behavior, will be observed when the restriction of spin is relaxed. In the system with spin the magnetic moments and spin susceptibility are of interest. Net magnetic moments seems to be roughly zero and absolute value of spin density might be appropriate.

$$\int d^3r \, \left| n^\uparrow (\boldsymbol{r}) - n^\downarrow (\boldsymbol{r}) \right| \tag{4.5}$$

The susceptibility along longitudinal can be calculated by using linear response theory for each sample. Careful treatment is necessary for taking ensemble average because of spin degree of freedom. Each sample can adopt a different spinor basis and the discussion about how to extract informations from the ensemble will be essential.

The compensation in doped semiconductors is also important factor in the metal-insulator transition. Suppose a system includes N_D donors and N_A acceptors satisfying $N_D > N_A$. Each donor impurity supplies one electron as the present study and each acceptor impurity absorbs one electron supplied by a donor impurity. Thus, each donor and acceptor have $+e$ and $-e$ net charge, respectively. This makes the system out of half-filling and randomness of the system becomes stronger. I expect qualitative differences in the compensated systems compared with the present study. Moreover, the study for the compensated system can be a perspective on whether the

agreement of μ in the uncompensated systems with narrow critical region with the compensated systems is by chance, or not [23].

Appendix A

Atomic units

Table A.1: Hartree atomic units. m_e, a_B, and e mean the electron mass, Bohr radius, and electron charge, respectively. The energy unit is called "Hartree". $\hbar$ is the Planck constant and ε_0 is the vacuum dielectric constant.

Mass	m_e	$9.10938188 \times 10^{-31}$[kg]
Length	$a_B \left(= \dfrac{4\pi\varepsilon_0 \hbar^2}{m_e e^2} \right)$	$5.291772108 \times 10^{-11}$[m]
Energy	$\dfrac{\hbar^2}{m_e a_B^2}$	$4.359744027 \times 10^{-18}$[J]
Charge	e	$1.60217646 \times 10^{-19}$[C]

Hamiltonian in an effective medium including single electron and impurity ion at $\boldsymbol{r}$ and $\boldsymbol{R}$, respectively, can be expressed as,

$$\mathcal{H}' = -\frac{\hbar^2}{2m_e^*}\nabla^2 - \frac{e^2}{4\pi\varepsilon_0\varepsilon_r}\frac{1}{|\boldsymbol{r}-\boldsymbol{R}|} \tag{A.1}$$

where ε_r is a dielectric constant of the effective medium. Eq. (A.1) is rewritten in the atomic units as,

$$\mathcal{H} = -\frac{1}{2m_e^*}\nabla^2 - \frac{1}{\varepsilon_r}\frac{1}{|\boldsymbol{r}-\boldsymbol{R}|} \tag{A.2}$$

Here I use m_e^* as a "relative" effective mass in the effective medium. m_e^* is conventionally used as an effective mass and I should use m_e^*/m_e instead of m_e^* in Eq. (A.2). Since m_e is 1 in the atomic units, I neglect the difference in the present article.

Appendix B

Electronic states in semiconductors

Purpose of this chapter is to introduce a description for an electronic state with doping a donor impurity in a semiconductor. The calculation described below follows that given in Ref. [26].

B.1 Effective mass approximation

Suppose a valence band is fully occupied by electrons at zero temperature in a semiconductor. The electronic states $\psi_{n,k}$ can be described as

$$\mathcal{H}^{(0)} \, \psi_{n,\boldsymbol{k}}^{(0)} = \epsilon_{n,\boldsymbol{k}}^{(0)} \, \psi_{n,\boldsymbol{k}}^{(0)} \tag{B.1}$$

where $\mathcal{H}^{(0)}$ is a Hamiltonian for the electrons, n is a band index and $\boldsymbol{k}$ is a Bloch wave number. I assume existence of a function w_n which satisfies

$$\psi_{n,\boldsymbol{k}}^{(0)} = \frac{1}{\sqrt{N_{\text{host}}}} \sum_{\boldsymbol{a}} e^{i\boldsymbol{k}\cdot\boldsymbol{a}} \, w_n \left(\boldsymbol{r} - \boldsymbol{a}\right) \tag{B.2}$$

where N_{host} is a number of atoms and $\boldsymbol{a}$ is a crystal lattice vector in a pure host semiconductor. The function w_n is called Wannier function. From the definition of w_n it can be expressed using $\psi_{n,\boldsymbol{k}}^{(0)}$.

$$w_n \left(\boldsymbol{r} - \boldsymbol{a}\right) = \frac{1}{\sqrt{N_{\text{host}}}} \sum_{\boldsymbol{k}} e^{-i\boldsymbol{k}\cdot\boldsymbol{a}} \, \psi_{n,\boldsymbol{k}}^{(0)} \tag{B.3}$$

Moreover one can derive a relationship below.

$$\int d^3r \; w_n^* \left(\boldsymbol{r} - \boldsymbol{a}\right) \psi_{n',\boldsymbol{k}}^{(0)} \left(\boldsymbol{r}\right) = \frac{1}{\sqrt{N_{\text{host}}}} \; \delta_{n,n'} \; e^{i\boldsymbol{k}\cdot\boldsymbol{a}} \qquad (\text{B.4})$$

Suppose a donor impurity is doped in this system. I consider about a perturbation given by the donor impurity ion. An electron interacts with the donor impurity ion through U which is screened by the host medium. The Schrödinger equation is

$$\left(\mathcal{H}^{(0)} + U\right) \psi = \epsilon \, \psi \qquad (\text{B.5})$$

I assume ψ is written as

$$\psi = \sum_{n,\boldsymbol{a}} f_n \left(\boldsymbol{a}\right) \; w_n \left(\boldsymbol{r} - \boldsymbol{a}\right) \qquad (\text{B.6})$$

and multiply $w_n^* \left(\boldsymbol{r} - \boldsymbol{a}\right)$ to Eq. (B.5) and integrate over the system.

$$\int d^3r \; w_n^* \left(\boldsymbol{r} - \boldsymbol{a}\right) \left(\mathcal{H}^{(0)} + U\right) \sum_{n',\boldsymbol{a}'} w_{n'} \left(\boldsymbol{r} - \boldsymbol{a}'\right) f_{n'} \left(\boldsymbol{a}'\right) = \epsilon \, f_n \left(\boldsymbol{a}\right) \qquad (\text{B.7})$$

here,

$$\sum_{n',\boldsymbol{a}'} \int d^3r \; w_n^* \left(\boldsymbol{r} - \boldsymbol{a}\right) \mathcal{H}^{(0)} w_{n'} \left(\boldsymbol{r} - \boldsymbol{a}'\right) f_{n'} \left(\boldsymbol{a}'\right)$$

$$= \sum_{n',\boldsymbol{a}'} \int d^3r \; w_n^* \left(\boldsymbol{r} - \boldsymbol{a}\right) \mathcal{H}^{(0)} \frac{1}{\sqrt{N_{\text{host}}}} \sum_{\boldsymbol{k}} e^{-i\boldsymbol{k}\cdot\boldsymbol{a}'} \; \psi_{n',\boldsymbol{k}} \left(\boldsymbol{r}\right) f_{n'} \left(\boldsymbol{a}'\right)$$

$$= \frac{1}{\sqrt{N_{\text{host}}}} \sum_{n',\boldsymbol{a}',\boldsymbol{k}} \epsilon_{n',\boldsymbol{k}}^{(0)} e^{-i\boldsymbol{k}\cdot\boldsymbol{a}'} \; f_{n'} \left(\boldsymbol{a}'\right) \int d^3r \; w_n^* \left(\boldsymbol{r} - \boldsymbol{a}\right) \psi_{n',\boldsymbol{k}} \left(\boldsymbol{r}\right)$$

$$= \frac{1}{N_{\text{host}}} \sum_{n',\boldsymbol{a}',\boldsymbol{k}} \epsilon_{n',\boldsymbol{k}}^{(0)} e^{-i\boldsymbol{k}\cdot(\boldsymbol{a}'-\boldsymbol{a})} \; f_{n'} \left(\boldsymbol{a}'\right) \delta_{n,n'}$$

$$= \sum_{\boldsymbol{a}'} \epsilon_{n,\boldsymbol{a}'-\boldsymbol{a}}^{(0)} \; f_n \left(\boldsymbol{a}'\right) \qquad (\text{B.8})$$

where $\epsilon_{n,\boldsymbol{a}}^{(0)}$ is a Fourier component of $\epsilon_{n,\boldsymbol{k}}^{(0)}$.

$$\epsilon_{n,\boldsymbol{a}}^{(0)} = \frac{1}{N_{\text{host}}} \sum_{\boldsymbol{k}} \epsilon_{n,\boldsymbol{k}}^{(0)} e^{-i\boldsymbol{k}\cdot\boldsymbol{a}} \qquad (\text{B.9})$$

Suppose a term $\epsilon^{(0)}_{n,\boldsymbol{k}} f_n$ and replace $\boldsymbol{k}$ by $-i\nabla$ in $\epsilon^{(0)}_{n,\boldsymbol{k}}$,

$$
\begin{aligned}
\epsilon^{(0)}_{n,-i\nabla} f_n(\boldsymbol{a}) &= \sum_{\boldsymbol{a'}-\boldsymbol{a}} \epsilon^{(0)}_{n,\boldsymbol{a'}-\boldsymbol{a}}\, e^{i(\boldsymbol{a'}-\boldsymbol{a})\cdot(-i\nabla)}\, f_n(\boldsymbol{a}) \\
&= \sum_{\boldsymbol{a'}} \epsilon^{(0)}_{n,\boldsymbol{a'}-\boldsymbol{a}}\, f_n(\boldsymbol{a'})
\end{aligned}
\tag{B.10}
$$

Using Eqs. (B.8), (B.9) and (B.10), Eq. (B.7) is

$$
\epsilon^{(0)}_{n,-i\nabla}\, f_n(\boldsymbol{a}) + \sum_{n',\boldsymbol{a'}} U_{n,n'}(\boldsymbol{a},\boldsymbol{a'})\, f_{n'}(\boldsymbol{a'}) = \epsilon\, f_n(\boldsymbol{a})
\tag{B.11}
$$

where

$$
U_{n,n'}(\boldsymbol{a},\boldsymbol{a'}) \equiv \int d^3r\, w_n^*(\boldsymbol{r}-\boldsymbol{a})\, U(\boldsymbol{r})\, w_{n'}(\boldsymbol{r}-\boldsymbol{a'})
\tag{B.12}
$$

I assume that an electron supplied from the donor will occupy a state at the bottom of conduction band of the host semiconductor. The energy origin is set at the bottom level of the conduction band. $\epsilon^{(0)}_{n,\boldsymbol{k}}$ can be approximated as

$$
\epsilon^{(0)}_{n,\boldsymbol{k}} \simeq \frac{1}{2m_e^*} k^2
\tag{B.13}
$$

where m_e^* is electron effective mass in the host semiconductor. (I should write m_e^*/m_e instead of just m_e^* but I omit the division by the electron mass because it is 1 in the atomic units.) And I assume U is enough smooth such that

$$
\begin{aligned}
U_{n,n'}(\boldsymbol{a},\boldsymbol{a'}) &\simeq U(\boldsymbol{a}) \int d^3r\, w_n^*(\boldsymbol{r}-\boldsymbol{a})\, w_{n'}(\boldsymbol{r}-\boldsymbol{a'}) \tag{B.14} \\
&= U(\boldsymbol{a})\, \delta_{\boldsymbol{a},\boldsymbol{a'}} \delta_{n,n'} \tag{B.15}
\end{aligned}
$$

Eventually, Eq. (B.11) becomes analogous to Schrödinger equation.

$$
\left(-\frac{1}{2m_e^*}\nabla^2 + U(\boldsymbol{r}) \right) f_n(\boldsymbol{r}) = \epsilon\, f_n(\boldsymbol{r})
\tag{B.16}
$$

B.2 Screened Coulomb interaction in semiconductors

Since I want to concentrate only on the electron supplied from the donor impurity, $U(\boldsymbol{r})$ should be an effective interaction which includes the true

interaction due to the impurity ion and screening given by electrons in the host semiconductor. The interaction between the additional electron and host electrons is assumed as a classical static Coulomb interaction. Then, a Fourier component of $U(r)$ can be expressed as

$$U\left(\boldsymbol{q}\right) = \frac{1}{\varepsilon_r\left(\boldsymbol{q}\right)}U_0\left(\boldsymbol{q}\right) \tag{B.17}$$

where $U_0(\boldsymbol{r})$ is the true interaction due to the impurity ion. $\varepsilon_r(\boldsymbol{q})$ is a dielectric function. $\varepsilon_r(\boldsymbol{q})$ can be expressed as

$$\frac{1}{\varepsilon_r\left(\boldsymbol{q}\right)} = 1 + \frac{4\pi}{q^2}\chi\left(\boldsymbol{q}\right) \tag{B.18}$$

where $\chi(\boldsymbol{q})$ is a density response function which is defined as,

$$\delta\rho\left(\boldsymbol{q}\right) = \chi\left(\boldsymbol{q}\right)U_0\left(\boldsymbol{q}\right) \tag{B.19}$$

where $\delta\rho$ is a density induced by the impurity ion. One can calculate $\chi(\boldsymbol{q})$ from linear response theory. In semiconductors this is roughly estimated in Ref. [26]

$$\chi\left(\boldsymbol{q}\right) \simeq \frac{n_v q^2}{m_e E_g^2} \tag{B.20}$$

where n_v is a number density of valence electrons. E_g is a band gap energy. From Eq. (B.18) and Eq. (B.20), $\varepsilon_r(\boldsymbol{q})$ becomes a constant and $U(\boldsymbol{r})$ is rewritten as

$$U\left(\boldsymbol{r}\right) = \frac{1}{\varepsilon_r}U_0\left(\boldsymbol{r}\right) \tag{B.21}$$

Appendix C

Real space finite difference approximation

Laplacian operator in Eq. (2.45) can be approximated by discretization of a function.

$$\nabla^2 f(x) = \frac{1}{a^2} \sum_{m=-M}^{M} c_m f(x + ma) + O(a^{2M}) \qquad (C.1)$$

a is a finite grid spacing and M is a cutoff order of the discretization. The sets of coefficients $\{c_m\}$ depend on M. These coefficients are shown in Table C.1 [59]. Here I mentioned only 1-dimensional case but the description in this chapter can be easily generalized for higher dimensional cases.

I checked accuracy of this approximation with respect to the order of finite difference approximation and the grid spacing. In this test calculations I set $m_e^* = \varepsilon_r = 1.0$. Fig. C.1 and C.3 are a calculation for a simple cubic hydrogen crystal that one hydrogen atom is in a unit cell. Fig. C.2 and C.4 are a calculation for the same unit cell as the case of Fig. C.1 and C.3 but the unit cell has two hydrogen atoms and these hydrogens align along x-direction like wires.

One might expect that the error shown in Fig. C.1 follows as a^{2M} but it is not correct. The point charge density is expressed as delta function, however, delta function is smoothed in the present calculations and the smoothing depends on the grid spacing (see Appendix D). The potentials for each grid spacing are not same despite they go to the same result asymptotically. The

same description can be applied to Fig. C.2. Fig. C.3 shows the dependence of total energy with respect to the order of finite difference approximation. The error in Fig. C.3 follows a^{2M}. There is difference among them only due to the approximation for Laplacian. Same dependence can be observed in Fig. C.4. Fig. C.5 and C.6 show the grid spacing dependence of square of Kohn-Sham orbital for the case of single particle and two particles, respectively. The results are calculated using the second order approximation for Laplacian. The error is comparably large near the hydrogen ions but negligible far from the ions. Fig. C.7 and C.8 show the square of Kohn-Sham orbital along x-axis for different order approximations about Laplacian. The first order results have large error and the higher order results show good convergence.

Even though there is quantitative error caused by finite difference approximation for differentiation but these results show qualitative similarity. If the order of approximation and the grid spacing are fixed for whole calculations one can expect reliable results are obtained.

Table C.1: The coefficients up to 4th order of finite difference approximation are shown below.

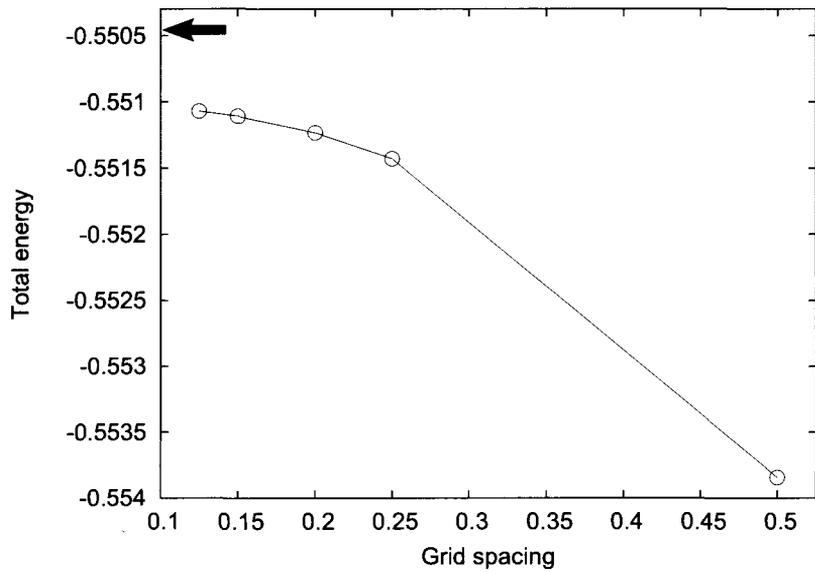| Order	c_0	$c_{\pm 1}$	$c_{\pm 2}$	$c_{\pm 3}$	$c_{\pm 4}$
1st	-2	1	0	0	0
2nd	$-\dfrac{5}{2}$	$\dfrac{4}{3}$	$-\dfrac{1}{12}$	0	0
3rd	$-\dfrac{49}{18}$	$\dfrac{3}{2}$	$-\dfrac{3}{20}$	$\dfrac{1}{90}$	0
4th	$-\dfrac{205}{72}$	$\dfrac{8}{5}$	$-\dfrac{1}{5}$	$\dfrac{8}{315}$	$-\dfrac{1}{560}$

Figure C.1: The grid spacing dependence for the total energy. This figure is for $L = 6$ Bohr, $N = 1$, and $M = 2$. The arrow indicates a result of KKR-Green's function method [60].
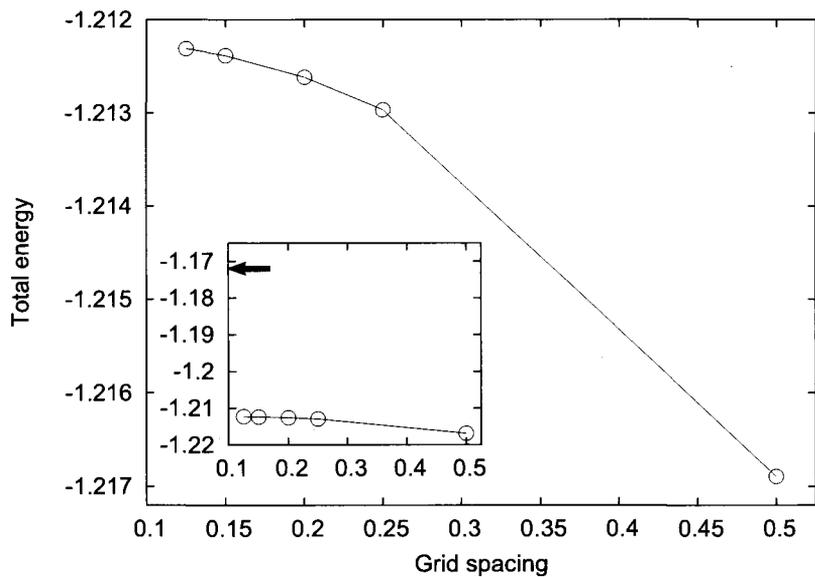

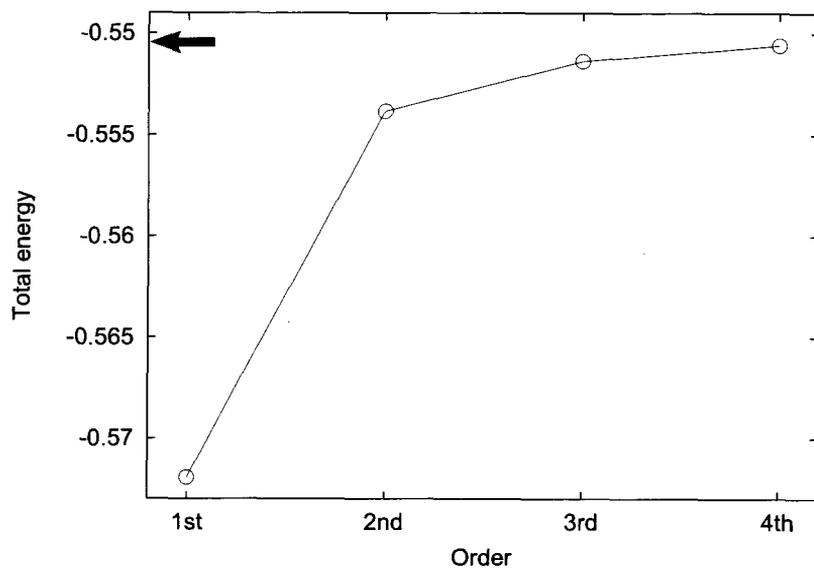Figure C.2: The grid spacing dependence for the total energy. This figure is for $L = 6$ Bohr, $N = 2$, and $M = 2$.

Figure C.3: The order of finite difference approximation dependence for the total energy. This figure is for $L = 6$ Bohr, $N = 1$, and $a = 0.5$ Bohr.
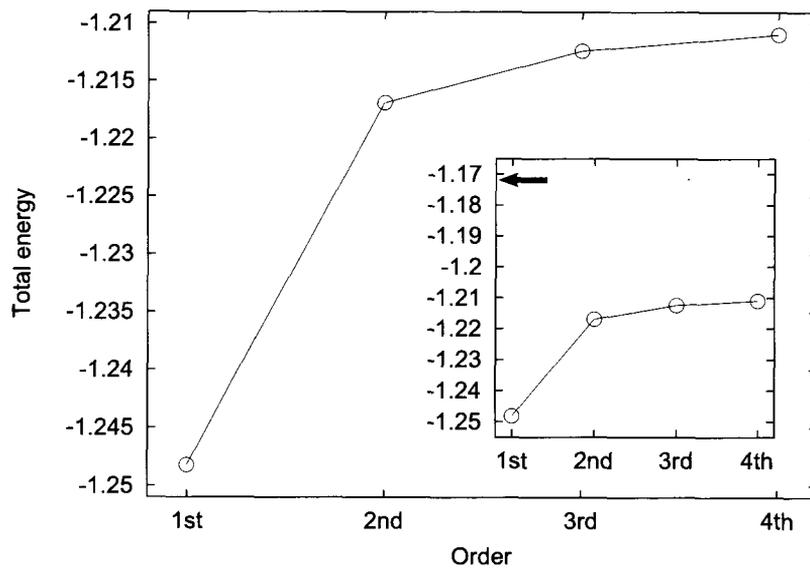

Figure C.4: The order of finite difference approximation dependence for the total energy. This figure is for $L = 6$ Bohr, $N = 2$, and $a = 0.5$ Bohr.
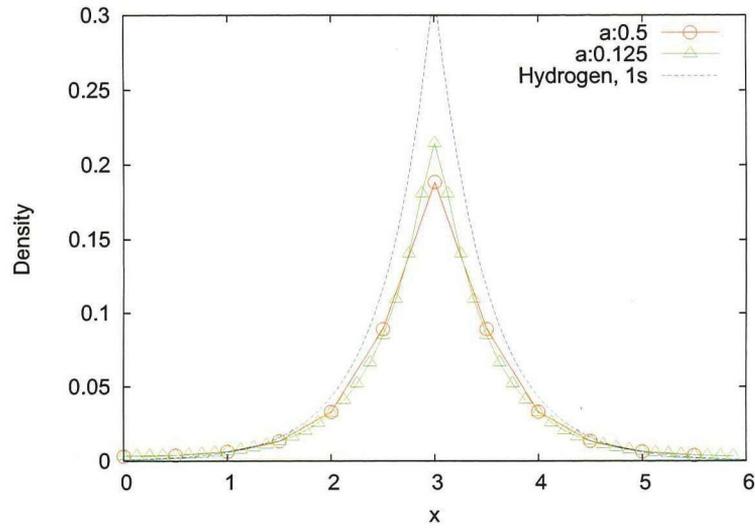
68

Figure C.5: The grid spacing dependence for $|\phi|^2$ along x-axis is shown. The impurity ion is put at $x = 3.0$. This figure is for $L = 6$ Bohr, $N = 1$, and $M = 2$. The dashed line is the Hydrogen 1s state.
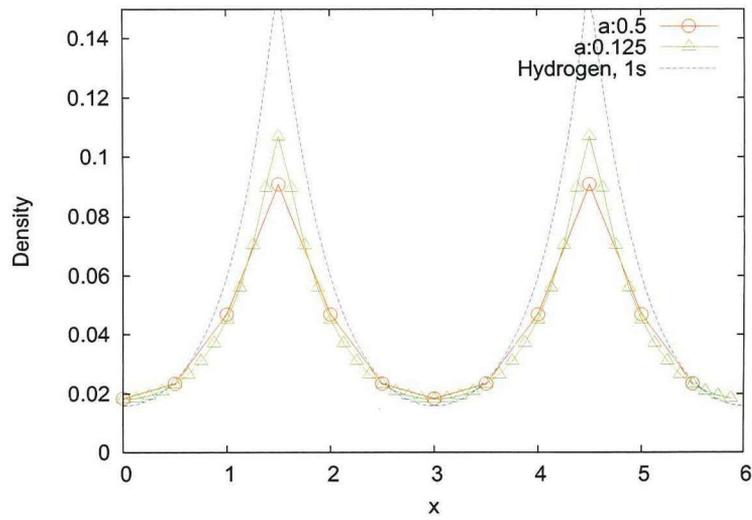

Figure C.6: The grid spacing dependence for $|\phi|^2$ along x-axis is shown. The impurity ion is put at $x = 1.5$ and 4.5. This figure is for $L = 6$ Bohr, $N = 2$, and $M = 2$. The dashed line corresponds to a linear combination of the Hydrogen 1s state density.
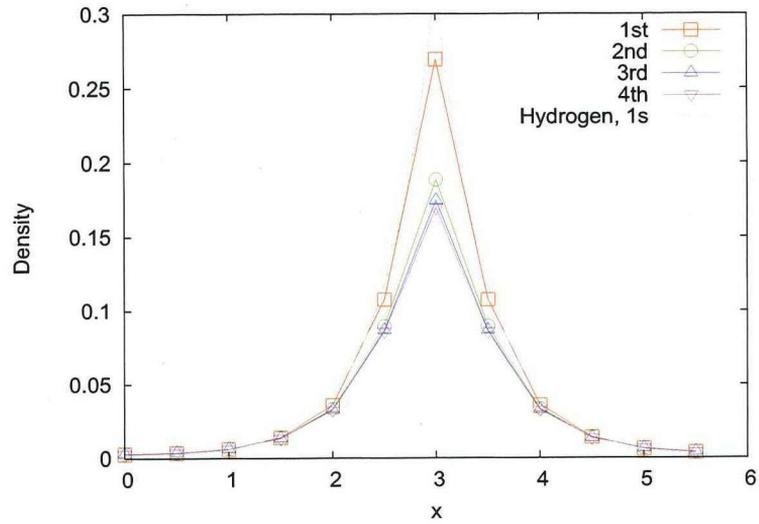
Figure C.7: The order of finite difference approximation dependence for $|\phi|^2$ along x-axis is shown. The impurity ion is put at $x = 3.0$. This figure is for $L = 6$ Bohr, $N = 1$, and $a = 0.5$ Bohr. The dashed line is for the Hydrogen 1s state.
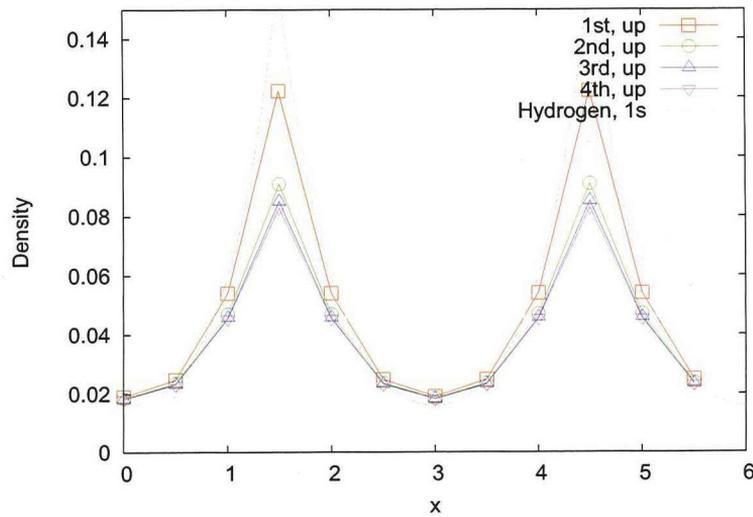

Figure C.8: The order of finite difference approximation dependence for $|\phi|^2$ along x-axis is shown. The impurity ion is put at $x = 1.5$ and $= 4.5$. This figure is for $L = 6$ Bohr, $N = 2$, and $a = 0.5$ Bohr. The dashed line corresponds to a linear combination of the Hydrogen 1s state density.

70

Appendix D

Poisson equation with periodic boundary condition

To solve Kohn-Sham equations Eqs. (2.45) and (2.46) one has to evaluate the Coulomb potential due to impurity ions and the Hartree potential.

$$\Phi(\boldsymbol{r}) = \int d^3r' \, \frac{\rho(\boldsymbol{r}')}{|\boldsymbol{r} - \boldsymbol{r}'|} \tag{D.1}$$

Each case in Eq. (2.46) corresponds below.

$$V_{\text{ext}}(\boldsymbol{r}) : -\Phi(\boldsymbol{r}) \quad , \quad \rho(\boldsymbol{r}) : \sum_I \delta(\boldsymbol{r} - \boldsymbol{R}_I) \tag{D.2}$$

$$V_{\text{Hartree}}(\boldsymbol{r}) : -\Phi(\boldsymbol{r}) \quad , \quad \rho(\boldsymbol{r}) : -n(\boldsymbol{r}) \tag{D.3}$$

Evaluation of the integration Eq. (D.1) can be replaced with solving Poisson equation.

$$-\Delta\Phi(\boldsymbol{r}) = 4\pi \, \rho(\boldsymbol{r}) \tag{D.4}$$

Within periodic boundary conditions one can express the charge density as a Fourier series.

$$\rho(\boldsymbol{r}) = \sum_k \rho_{\boldsymbol{k}} e^{i\boldsymbol{k}\cdot\boldsymbol{r}} \tag{D.5}$$

where $\boldsymbol{k}$ is restricted by the boundary conditions.

$$(k_x, k_y, k_z) = \frac{2\pi}{L}(n_x, n_y, n_z) \quad , \quad (n_{x,y,z} = 0, \pm 1, \pm 2, \cdots) \tag{D.6}$$

Here $\boldsymbol{k} = \boldsymbol{0}$ means a constant contribution to the potential and it is removed by hand assuming that the neutrality is satisfied. The potential is also expanded as the Fourier series.

$$\Phi(\boldsymbol{r}) = \sum_{k} \Phi_{\boldsymbol{k}} e^{i\boldsymbol{k}\cdot\boldsymbol{r}} \tag{D.7}$$

An relationship for these Fourier components can be derived from Eq. (D.4).

$$\Phi_{\boldsymbol{k}} = \frac{4\pi}{k^2} \rho_{\boldsymbol{k}} \tag{D.8}$$

For numerical purposes a cut-off is imposed on the wavenumbers so that the number of terms in the Fourier series is equal to the number of points of the real-space grid. Both density and potentials in real space must be a real number.

$$\rho(\boldsymbol{r}) = \rho(\boldsymbol{r})^* \tag{D.9}$$

$$\Phi(\boldsymbol{r}) = \Phi(\boldsymbol{r})^* \tag{D.10}$$

Thus, the Fourier components must satisfy,

$$\rho_{\boldsymbol{k}} = \rho^*_{-\boldsymbol{k}} \tag{D.11}$$

$$\Phi_{\boldsymbol{k}} = \Phi^*_{-\boldsymbol{k}} \tag{D.12}$$

The Fourier transformation used in numerical analysis is usually implemented with $n_{x,y,z} = (0, \cdots, L/a - 1)$ for Eq. (D.6). However, I shift the indices to satisfy Eqs. (D.11) and (D.12).

$$n_{x,y,z} = -\left\lfloor \frac{1}{2}\left(\frac{L}{a} - 1\right) \right\rfloor, \cdots, \left\lfloor \frac{L}{2a} \right\rfloor \tag{D.13}$$

where $\lfloor \ \rfloor$ is a floor function. This cut-off replaces the delta-functions of the charge density of the impurity ions with an approximate smooth charge density. Poisson equation is solved exactly for this approximate density and the corresponding potential obtained using an inverse Fourier transform.
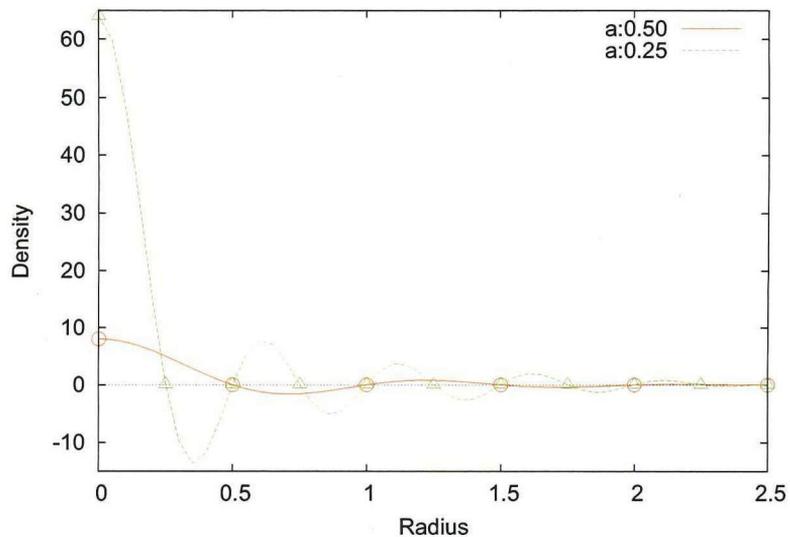
Figure D.1: The delta function is smoothed as shown above. Red and green lines are calculated with $a = 0.5$ Bohr and $a = 0.25$ Bohr in a periodic system with $L = 5.0$ Bohr, respectively. Red circles and green triangles show the data values on the real-space grid.
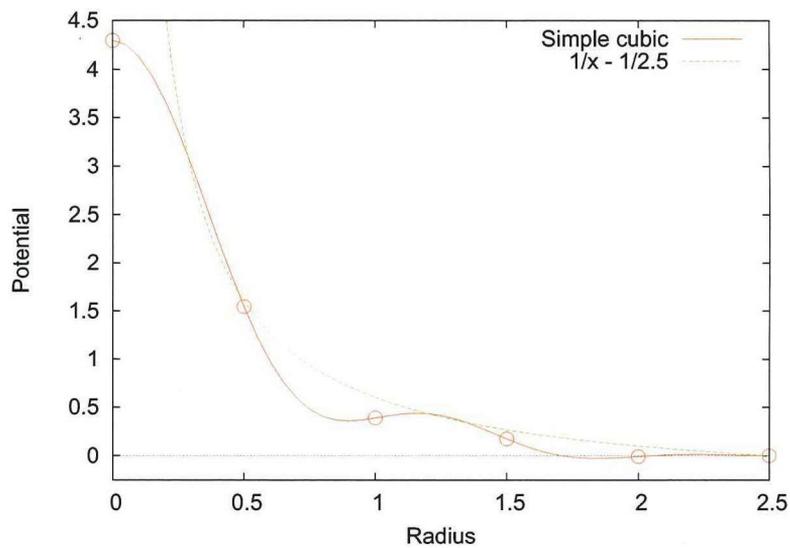

Figure D.2: The figure shows a result of Poisson equation for $L = 5.0$ Bohr and $a = 0.5$ Bohr. Circles show the data values on the real-space grid.
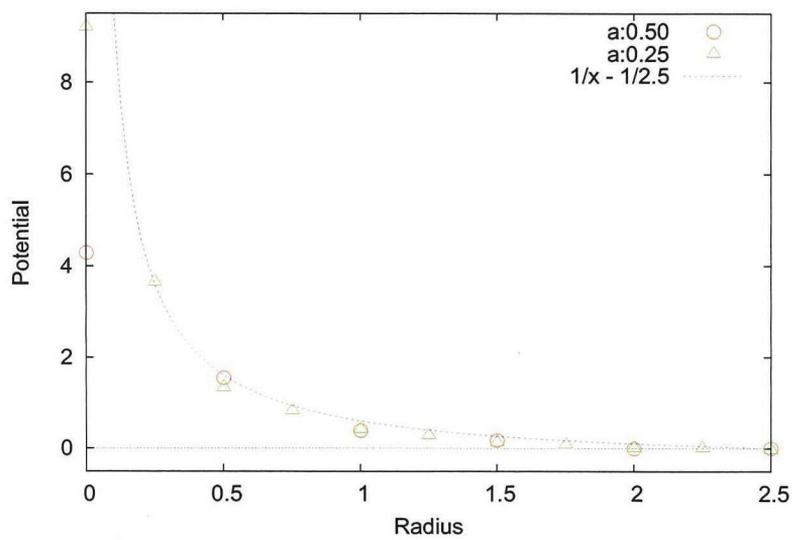
Figure D.3: Red and green points are corresponding to the result for $a = 0.5$ Bohr and $a = 0.25$ Bohr. The difference is clear especially near origin.

Acknowledgment

I would like to express my gratitude to Prof. Keith Slevin for his supervision. He gave me a lot of significant advices and valuable opportunities in his supervision and I really enjoyed this study. I also would like to thank Prof. Tetsuo Ogawa, Prof. Kensuke Kobayashi, Prof. Kazuhiko Kuroki, and Prof. Masako Ogura for their supervision through my PhD defense as the examination committee.

This study was supported in part by Global COE Program (Core Research and Engineering of Advanced Materials-Interdisciplinary Education Center for Materials Science), MEXT, Japan. I owe a very important debt to Prof. Yoshio Kitaoka, the project leader of the program.

I am deeply grateful to Prof. Hisazumi Akai for the fruitful discussion about this study. And I referred to his program code and his helpful advice to implement my program. I am indebted to Prof. Masaaki Geshi, Prof. Kenichi Asano, and Prof. Takuma Ohashi for their helpful advice. I also would like to thank Dr. Taro Fukazawa, Dr. Kouta Watanabe, and Dr. Kenji Kamide for giving me some opportunities to have helpful discussion.

I would like to appreciate Prof. Tomi Ohtsuki for the important indication and kind help. Some parts of the results in this study are calculated on the supercomputer at ISSP and the calculation was done as a part of his project. And I was so encouraged by his warm help. I also would like to appreciate Prof. Rudolf Römer for kind acceptance in the Center for Scientific Computing in University of Warwick. He gave me some basic concepts at the beginning of this work. This stay is supported from JSPS International Training Program (ITP). And I would like to appreciate Prof. Stefan Kettemann for his important suggestion about the perspective of this study. His advice created some outlooks of this study and I am so interested in his

point.

I thank Ms. Tomoko Shimokomaki and Yukiko Kajimoto for their support about paperwork in my research life. I also thank my colleagues, Mr. Shotaro Doi, Dr. Tetsuya Nagata, Mr. Ryosuke Saito, Ms. Ayaka Mashiyama, and Mr. Syo Iwasaki in Theory of electrons in solids group (former Akai group), and Dr. Koji Kobayashi in Sophia University for kind fellowship.

I am sorry for not introducing all the people who helped me. I hope their excuse.

Finally, I wish to thank my parents, Hisamitsu and Michiko Harashima for their kind support for my life.

Bibliography

[1] P. W. Anderson, Phys. Rev. **109**, 1492 (1958).

[2] B. Kramer and A. MacKinnon, Rep. Prog. Phys. **56**, 1469 (1993).

[3] F. Evers and A. D. Mirlin, Rev. Mod. Phys. **80**, 1355 (2008).

[4] E. Abrahams, *50 Years of Anderson Localization*, 1st ed. (World Scientific, Singapore, 2010).

[5] E. Abrahams, P. W. Anderson, D. C. Licciardello, and T. V. Ramakrishnan, Phys. Rev. Lett. **42**, 673 (1979).

[6] A. MacKinnon and B. Kramer, Phys. Rev. Lett. **47**, 1546 (1981).

[7] A. MacKinnon and B. Kramer, Zeitschrift für Physik B Condensed Matter **53**, 1 (1983).

[8] J. L. Pichard and G. Sarma, Journal of Physics C: Solid State Physics **14**, L127 (1981).

[9] K. Slevin and T. Ohtsuki, Phys. Rev. Lett. **78**, 4083 (1997).

[10] Y. Asada, K. Slevin, and T. Ohtsuki, Phys. Rev. Lett. **89**, 256601 (2002).

[11] K. Slevin and T. Ohtsuki, Phys. Rev. B **80**, 041304(R) (2009).

[12] K. Slevin and T. Ohtsuki, Phys. Rev. Lett. **82**, 382 (1999).

[13] K. Slevin, T. Ohtsuki, and T. Kawarabayashi, Phys. Rev. Lett. **84**, 3915 (2000).

[14] L. J. Vasquez, A. Rodriguez, and R. A. Römer, Phys. Rev. B **78**, 195106 (2008).

[15] A. Rodriguez, L. J. Vasquez, and R. A. Römer, Phys. Rev. B **78**, 195107 (2008).

[16] A. Rodriguez, L. J. Vasquez, K. Slevin, and R. A. Römer, Phys. Rev. Lett. **105**, 046403 (2010).

[17] A. Rodriguez, L. J. Vasquez, K. Slevin, and R. A. Römer, Phys. Rev. B **84**, 134209 (2011).

[18] T. F. Rosenbaum, K. Andres, G. A. Thomas, and R. N. Bhatt, Phys. Rev. Lett. **45**, 1723 (1980).

[19] H. Stupp, M. Hornung, M. Lakner, O. Madel, and H. v. Löhneysen, Phys. Rev. Lett. **71**, 2634 (1993).

[20] F. J. Wegner, Zeitschrift för Physik B Condensed Matter **25**, 327 (1976), 10.1007/BF01315248.

[21] M. A. Paalanen, T. F. Rosenbaum, G. A. Thomas, and R. N. Bhatt, Phys. Rev. Lett. **48**, 1284 (1982).

[22] S. Waffenschmidt, C. Pfleiderer, and H. v. Löhneysen, Phys. Rev. Lett. **83**, 3005 (1999).

[23] K. M. Itoh, M. Watanabe, Y. Ootuka, E. E. Haller, and T. Ohtsuki, JPSJ **73**, 173 (2004).

[24] H. Löhneysen, Annalen der Physik **523**, 599 (2011).

[25] J. J. Krich and A. Aspuru-Guzik, Phys. Rev. Lett. **106**, 156405 (2011).

[26] J. M. Ziman, *Principles of the Theory of Solids*, 2nd ed. (Cambridge University Press, Cambridge, 1972).

[27] P. P. Edwards and M. J. Sienko, Phys. Rev. B **17**, 2575 (1978).

[28] N. F. Mott, *Metal-Insulator Transitions*, 2nd ed. (Taylor & Francis, London, 1990).

[29] J. H. Rose, H. B. Shore, and L. M. Sander, Phys. Rev. B **21**, 3037 (1980).

[30] R. N. Bhatt and T. M. Rice, Phys. Rev. B **23**, 1920 (1981).

[31] E. Ertekin, M. T. Winkler, D. Recht, A. J. Said, M. J. Aziz, T. Buonassisi, and J. C. Grossman, Phys. Rev. Lett. **108**, 026401 (2012).

[32] K. Andres, R. N. Bhatt, P. Goalwin, T. M. Rice, and R. E. Walstedt, Phys. Rev. B **24**, 244 (1981).

[33] A. L. Efros and B. I. Shklovskii, Journal of Physics C: Solid State Physics **8**, L49 (1975).

[34] T. F. Rosenbaum, K. Andres, G. A. Thomas, and P. A. Lee, Phys. Rev. Lett. **46**, 568 (1981).

[35] X. Liu, A. Sidorenko, S. Wagner, P. Ziegler, and H. v. Löhneysen, Phys. Rev. Lett. **77**, 3395 (1996).

[36] D. Belitz and T. R. Kirkpatrick, Rev. Mod. Phys. **66**, 261 (1994).

[37] P. Hohenberg and W. Kohn, Phys. Rev. **136**, B864 (1964).

[38] R. G. Parr and W. Yang, *Density-Functional Theory of Atoms and Molecules*, 1st ed. (Oxford University Press, Oxford, 1989).

[39] R. M. Martin, *Electronic Structure: Basic Theory and Practical Methods*, 1st paperback ed. (Cambridge University Press, Cambridge, 2008).

[40] W. Kohn and L. J. Sham, Phys. Rev. **140**, A1133 (1965).

[41] Y. Harashima and K. Slevin, International Journal of Modern Physics: Conference Series **11**, 90 (2012).

[42] W. Kohn, Phys. Rev. **105**, 509 (1957).

[43] W. Kohn, Phys. Rev. **110**, 857 (1958).

[44] O. Gunnarsson, B. I. Lundqvist, and J. W. Wilkins, Phys. Rev. B **10**, 1319 (1974).

[45] J. F. Janak, V. L. Moruzzi, and A. R. Williams, Phys. Rev. B **12**, 1257 (1975).

[46] L. Hedin, Phys. Rev. **139**, A796 (1965).

[47] W. H. Press, B. P. Flannery, S. A. Teukolsky, and W. T. Vetterling, *Numerical Recipes*, 2nd ed. (Cambridge University Press, Cambridge, 1992).

[48] M. Bollhfer and Y. Notay, Computer Physics Communications **177**, 951 (2007).

[49] A. Weiße, G. Wellein, A. Alvermann, and H. Fehske, Rev. Mod. Phys. **78**, 275 (2006).

[50] A. D. Mirlin, Y. V. Fyodorov, A. Mildenberger, and F. Evers, Phys. Rev. Lett. **97**, 046803 (2006).

[51] R. W. Godby and R. J. Needs, Phys. Rev. Lett. **62**, 1169 (1989).

[52] F. Aryasetiawan and O. Gunnarsson, Reports on Progress in Physics **61**, 237 (1998).

[53] G. Onida, L. Reining, and A. Rubio, Rev. Mod. Phys. **74**, 601 (2002).

[54] J. T. Edwards and D. J. .Thouless, Journal of Physics C: Solid State Physics **5**, 807 (1972).

[55] D. Braun, E. Hofstetter, A. MacKinnon, and G. Montambaux, Phys. Rev. B **55**, 7557 (1997).

[56] C.-O. Almbladh and U. von Barth, Phys. Rev. B **31**, 3231 (1985).

[57] W. Kohn, Phys. Rev. **133**, A171 (1964).

[58] M. Methfessel and J. Kubler, Journal of Physics F: Metal Physics **12**, 141 (1982).

[59] J. R. Chelikowsky, N. Troullier, K. Wu, and Y. Saad, Phys. Rev. B **50**, 11355 (1994).

[60] H. Akai, AkaiKKR, http://kkr.phys.sci.osaka-u.ac.jp/.